Large Force Range Mechanically Adjustable Dampers for Heavy Vehicle Applications

William C.T. Burke

Thesis submitted to the faculty of Virginia Polytechnic Institute and State University in partial fulfillment of the requirements for the degree of

Master of Science

In

Mechanical Engineering

Mehdi Ahmadian, Chair

Saied Taheri

Daniel J. Inman

June 1, 2010

Blacksburg, Virginia

Keywords: Electro-hydraulic Damper, Mechanically Adjustable Damper, Magneto-Rheological Damper, Heavy Truck

Large Force Range Mechanically Adjustable

Dampers for Heavy Vehicle Applications

William C.T. Burke

Abstract

Semi-active dampers utilizing various working principles have been developed for a variety of vehicles. These semi-active dampers have been designed to resolve the ride and handling compromise associated with conventional passive dampers, and increase vehicle stability. This thesis briefly reviews existing semi-active damper designs, including but not limited to MR dampers, before presenting two new prototype semi-active hydraulic dampers. Both prototype dampers are designed to provide a large force range while maintaining easily controllable valve characteristics.

The first of these dampers served primarily as a proof of concept and a means of understanding the dynamics of a disc valve housed inside the main piston. The valve design is presented, along with other information concerning the fabrication of the Initial Prototype damper. Test results are presented and analyzed, and a second iteration of the valve is designed. The Final Prototype damper is a scaled up version of the initial design, with refinements made in piston geometry, internal disc profile, and dynamic seals. This large force range damper is tested and results are compared with existing MR dampers. The Final Prototype damper provides a significantly larger force range when compared with typical MR dampers. Finally, to conclude this research, the vehicle dynamics implications of the Final Prototype damper are discussed and recommendations for further study are made.

Acknowledgements

I would like to thank Dr. Mehdi Ahmadian for his guidance throughout my work in the Masters of Science program. His patience and concern for each of his many students is remarkable. I would also like to thank Dr. Dan Inman and Dr. Saied Taheri for their participation as members of my graduate committee. To Alireza Farjoud and Michael Craft, many thanks are due for their assistance during testing and enjoyable company. To Clement Nagode, thank you for your constant willingness to discuss design ideas and your fresh eye. To Parham, thanks for your friendship and enlightening perspective. America is a good fit for you my friend, and I hope you stick around. To Sue Teel, thanks for helping me deal with finicky vendors and making sure my purchase orders went through on time. Thanks are also due to TACOM for their funding of this research.

Mom and Dad, I cannot thank you enough for caring about my education the way you have, and for supporting me along the way. I love you both. James, thanks for picking up the phone when I was up to my eyes in work and frustrated as hell. You are still the smartest guy I know, a great brother, and an even better friend.

To all my boys at 317 Clay Street, past and present, endless thanks for making life in a small mountain town seem sublime. Clay and John, good luck with your degrees, it'll be over before you know it.

To everyone from Richmond who I care about, you know who you are, thank you!

Contents

List of Tables

List of Figures

Chapter 1

Introduction

The purpose of this chapter is to orient the reader with the topic of semi-active devices as they relate to vehicle suspensions. Semi-active devices can be broken into two distinct categories: those that use smart materials, and those that do not. Both are computer controlled intelligent systems, yet their principles of operation differ. Smart material devices include electro-rheological and magneto-rheological (MR) fluids, Shape Memory Alloys, Piezoceramics, and any other material whose physical properties change in response to magnetic, electrical, or thermal stimulus. Semi-active devices that do not use smart materials instead use more conventional actuators to modify their output force. Common actuators include voice coils and solenoid valves, pneumatic or hydraulic cylinders, as well as stepper motors and servos.

1.1 A Broad Overview of Semi-active Devices

Early semi-active dampers were born out of the modification of conventional passive dampers. These dampers were modified such that the working fluid was diverted through a controllable one way valve. Typically, these valves modified the hydraulic flow area using a solenoid or voice coil type actuator acting on a spool proportioning valve. A good example of this type of semi-active damper can be found in the work of Kitching, et al. [12]. This style of damper has enjoyed reasonable commercial success. One such system is manufactured by ZF Sachs GmbH and marketed as their Continuous Damping Control (restricted) semi-active hydraulic damping system. Other semi-active damping solutions have been explored outside the realm of solenoid proportioning valves. Wolfe, et al. [13] developed and patented a bypass valve mounted concentrically in the main damper piston. This valve is designed to be actuated externally, either through a stepper motor, for continuously variable control, or a two position actuator, for on-off two state control.

Much of the research into smart material semi-active damping systems has been in MR devices. Though MR fluids were first discovered in the late 1940's, the majority of their

research and development has occurred after 1990 [7]. Lord Corporation has enjoyed commercial success with *Motion Master semi-active damping system*^{TM}, which is employed in seat suspensions in commercial trucks and prosthetic legs [14]. Many other researchers have shown the benefits of MR dampers in increased ride comfort, reduced body accelerations, and improved vehicle stability [5, 8, 10, 17].

1.2 Research Objectives

The primary objectives of this study are:

1. study existing semi-active damping solutions,
2. design, prototype, and develop a high force range mechanically adjustable hydraulic damper,
3. explore applications of this damper, vis-à-vis heavy vehicles, and
4. provide recommendations for the effective design and fabrication of a new generation of mechanically adjustable dampers.

1.3 Approach

During the course of this research, two main prototype dampers were developed. Both dampers were developed for automotive use; the first being primarily a proof of concept device and a tool for understanding the dominant mechanics of the design, the second being a more refined implementation of the valve design intended for larger vehicles and higher force applications. Many different valve geometries were prototyped and tested, with significant design milestones and refinements being highlighted in this document. Based on the characteristics of the prototype dampers, future design recommendations are made, in addition to highlighting applications where this type of damper might be most effective.

1.4 Outline

Chapter 2 briefly covers the technical background of suspensions and the corresponding effects on vehicle dynamics, as well as a review of the existing literature on semi-active dampers. Chapter 3 covers the design, fabrication, and characterization of the Initial Prototype Mechanically Adjustable Hydraulic Damper. Chapter 4 introduces the Final Prototype Mechanically Adjustable Hydraulic Damper. Two new disc valve designs are discussed and test results are presented in Chapter 5. Chapter 6 is a comparison of existing MR dampers with the dampers developed in this study, highlighting the differences in available force range and the implications for controls and vehicle stability. Chapter 7 gives a summary of the work that was completed and recommendations for future mechanically adjustable damper designs.

Chapter 2

Technical Background and Literature Review

The purpose of this chapter is to introduce the reader to the function of vehicle suspensions, with a particular focus on dampers. After a brief discussion on conventional passive dampers, two types of semi-active dampers are introduced: magnetorheological (MR) dampers and mechanically adjustable hydraulic dampers. The effect of primary suspensions on vehicle dynamics is discussed from the perspective of both ride and handling, as well as the trade-offs associated with passive dampers and semi-active control. Lastly, a review of existing literature is presented to familiarize the reader with the field of semi-active devices and their commercial applications.

2.1 Heavy Vehicle Suspensions

The primary purpose of a vehicle's suspension is to isolate the driver and occupants from disturbances and vibrations caused by road irregularities. In addition to vibration isolation, suspensions are designed to maintain vehicle stability and ensure sufficient responsiveness to driver inputs. A conventional passive suspension is composed of a spring and damper combination associated with each corner, or wheel of the vehicle. These springs and dampers may be coupled across a vehicle axle, as is the case with most heavy trucks, or actuated independently. In either case, each spring and damper pair works in series with the tire to isolate the chassis from all oscillatory modes: one wheel bump, heave, pitch, roll, and warp. To illustrate the basic mechanical layout of a vehicle suspension, a quarter car model is presented in Figure 2.1.

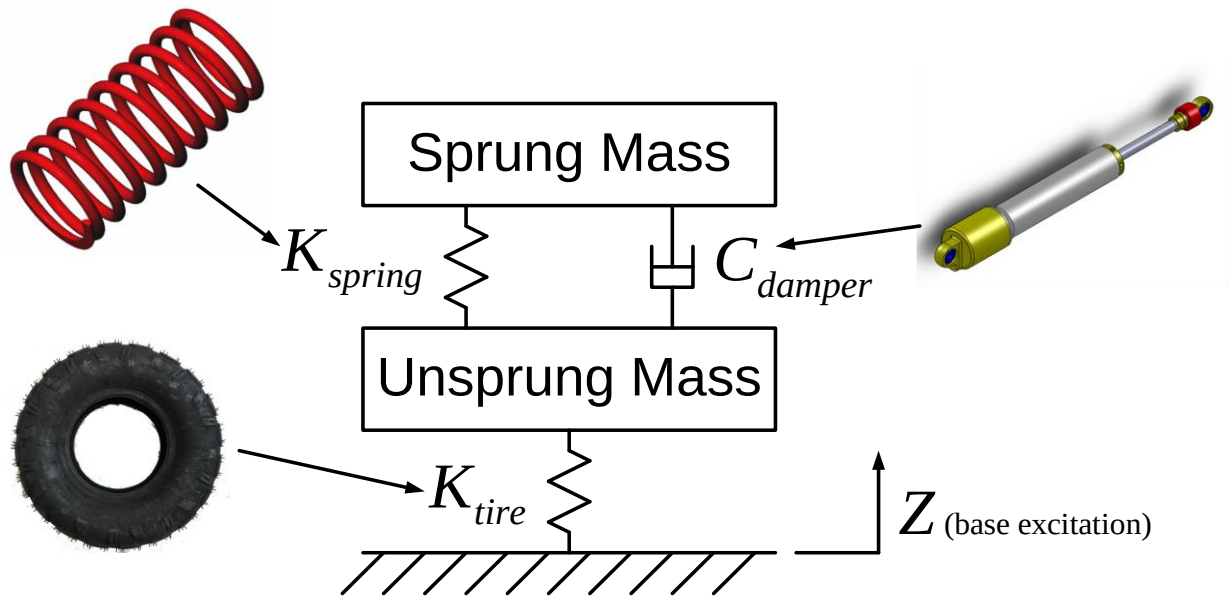

Figure 2.1 Quarter Car representation of vehicle suspension

2.2 Dampers

In the idealized quarter car model shown above in Figure 2.1, the damper is the only component capable of removing energy from the system and attenuating the sprung mass vibration due to base excitation. In general, conventional passive hydraulic dampers exert a force in the opposite direction of their motion, proportional to the velocity of their extension or compression. Different valve geometries and damper designs can change the relationship between damper force and velocity. In most cases however, damper force is approximately linear with respect to input velocity. This allows for the modeling of the damper force using a constant damping coefficient, which gives rise to a damping force that is a linear function of damper velocity. A linear representation of damping facilitates the development of simple equations of motion which, in many cases, can be solved for analytically.

In order to demonstrate the influence of dampers on sprung mass/chassis vibration, an even simpler single degree of freedom (SDOF) is presented in Figure 2.2. Ignoring the behavior of the unsprung mass in Figure 2.1 we can reduce the model of sprung mass dynamics to a single degree of freedom mass-spring-damper subject to a harmonic base excitation $y(t) = Y \sin \omega_b t$.

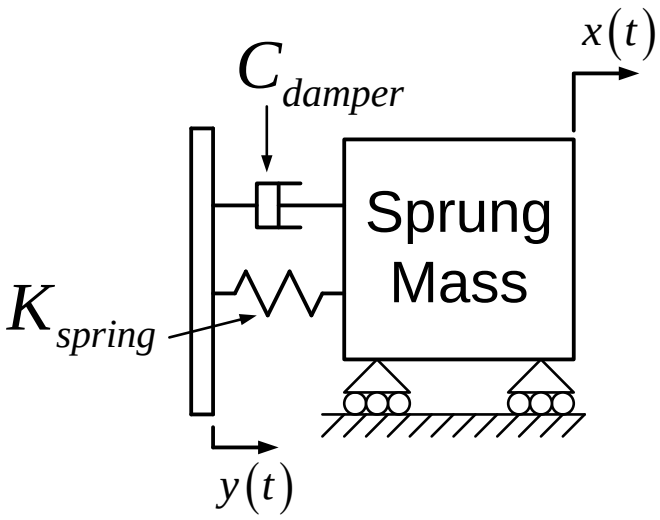

Figure 2.2 S.D.O.F. base excitation model

A force balance yields

$$m_{sprung}\ddot{x} + c_{damper}\left(\dot{x} - \dot{y}\right) + k_{spring}\left(x - y\right) = 0 \tag{2-1}$$

where k_{spring} and c_{damper} represent the spring constant and damping coefficient respectively. It is assumed that the base experiences harmonic motion, represented by

$$y(t) = Y \sin \omega_b t \tag{2-2}$$

where Y and ω_b represent the amplitude of the base motion and the frequency of base oscillation, respectively. Combining equations (2-2) and (2-1), then dividing by m yields

$$\ddot{x} + 2\zeta\omega_n\dot{x} + \omega_n^2 x = 2\zeta\omega_n\omega_b Y \cos\omega_b t + \omega_n^2 Y \sin\omega_b t \tag{2-3}$$

where ω_n is the sprung mass natural frequency, ω_b represents the base excitation frequency, and ζ denotes the damping ratio, where $\zeta = \dfrac{c_{damper}}{2\sqrt{k_{spring}/m_{sprung}}}$. Solving by using the linearity of equation (2-3) and the principal of superposition yields

$$x_p(t) = \omega_n Y \left[\frac{\omega_n^2 + (2\zeta\omega_b)^2}{(\omega_n^2 - \omega_b^2)^2 + (2\zeta\omega_n\omega_b)^2} \right]^{\frac{1}{2}} \cos(\omega_b t - \phi_1 - \phi_2) \tag{2-4}$$

where

$$\phi_1 = \tan^{-1} \frac{2\zeta\omega_n\omega_b}{\omega_n^2 - \omega_b^2} \tag{2-5}$$

and

$$\phi_2 = \tan^{-1} \frac{\omega_n}{2\zeta\omega_b} \tag{2-6}$$

Substituting equations (2-5) and (2-6) into equation (2-4) yields the following normalized representation of our SDOF system

$$\frac{X}{Y} = \left[\frac{1 + (2\zeta r)^2}{(1 - r^2)^2 + (2\zeta r)^2} \right] \tag{2-7}$$

where frequency ratio $r = \omega_b / \omega_n$.

Plotting the displacement ratio X/Y versus frequency ratio at various values of ζ gives a graphical representation of the response of the sprung mass as a function of damping and input frequency.

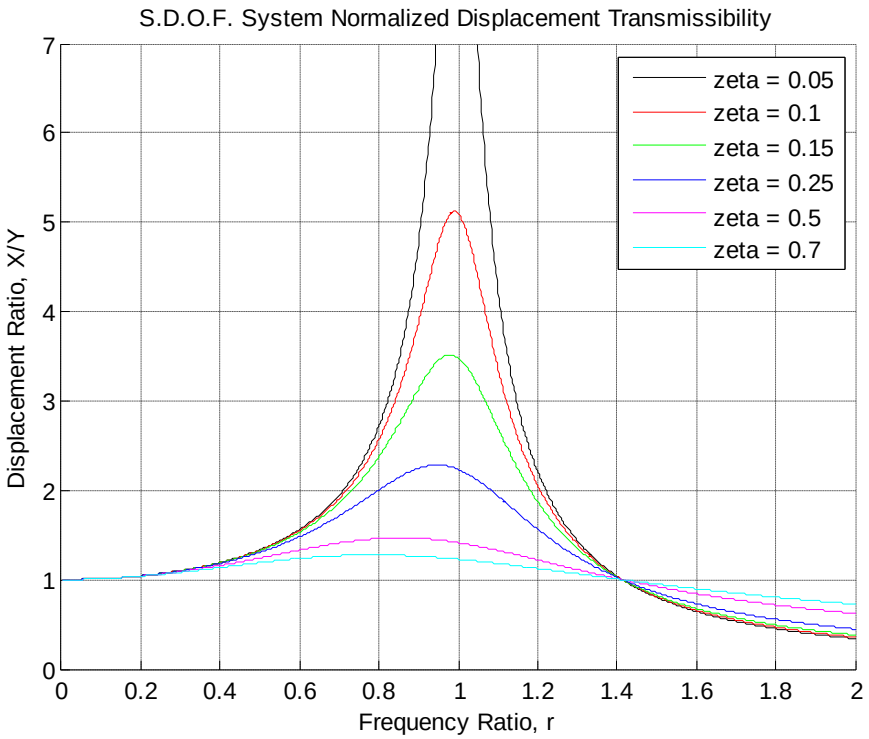

Figure 2.3 Displacement Transmissibility as a function of frequency for various ζ values

The first important thing to note about Figure 2.3 is the crossover point at $r = \sqrt{2}$. For $r < \sqrt{2}$ the sprung mass exhibits oscillations with a larger amplitude than that of the base excitation for all values of ζ. The influence of the damping ratio ζ on the amplitude of the sprung mass vibrations is no less important, particularly as the driving frequency approaches the natural frequency of the sprung mass $\left(\omega_b \to \omega_n \text{ ie., } r \to 1\right)$. For $r < \sqrt{2}$ increasing ζ causes a reduction in the amplitude of the sprung mass oscillation, while for $r > \sqrt{2}$ increasing ζ tends to cause the opposite effect, yielding an increase in the amplitude of sprung mass oscillation [1]. Understanding the frequency dependence of displacement and force transmissibility is of paramount importance to the passive hydraulic damper designer and is the basis for understanding the compromise between ride and handling. The nature of this compromise, the disadvantages of passive dampers, and the semi-active approach to controlling vehicle dynamics are explained more thoroughly in the following section.

2.3 Effect of Suspension on Vehicle Dynamics

This section will briefly discuss the primary effects of suspension systems on vehicle dynamics. For readers more interested in passive dampers specifically, consult Dixon [2]. For a detailed introduction to tire mechanics, the nature of suspension input forces, vehicle dynamics, and much more see Milliken [4] and Dixon [3].

2.3.1 Ride vs. Handling

The ride versus handling compromise is predominantly a function of the passive hydraulic damper's inability to handle all frequencies of road inputs optimally, and the competing needs of the tires and chassis. Ignoring the tire for the time being and returning to Figure 2.3, it is evident that the passive damper is incapable of optimally attenuating sprung mass oscillations for all input frequencies.

Take for example, a heavy truck with a heave natural frequency $\omega_{heave} = 1.8Hz$. In order to reduce the chassis motion due to lower frequency inputs, such as road undulations, $\zeta = 0.7$ would be desirable. For excitations above ω_{heave}, such as one wheel bump at highway speed due to a pothole or pavement irregularity, $\zeta = 0.7$ would cause an increase in chassis motion and disturbance to the driver. Damping ratio has a dominant effect on the forces experienced by the chassis, most clearly demonstrated by analyzing the force transmissibility of the SDOF model presented in Section 2.2. Differentiating equation (2-4) twice and applying Newton's second law yields the following expression for force transmissibility

$$\frac{F_T}{kY} = r^2 \left[\frac{1+(2\zeta r)^2}{(1-r^2)^2+(2\zeta r)^2} \right]^{\frac{1}{2}} \tag{2-8}$$

where F_T/kY is a dimensionless representation of the force magnitude applied to the sprung mass due to displacement Y in the base amplitude. A more detailed derivation of (2-8) can be found in Inman [1].

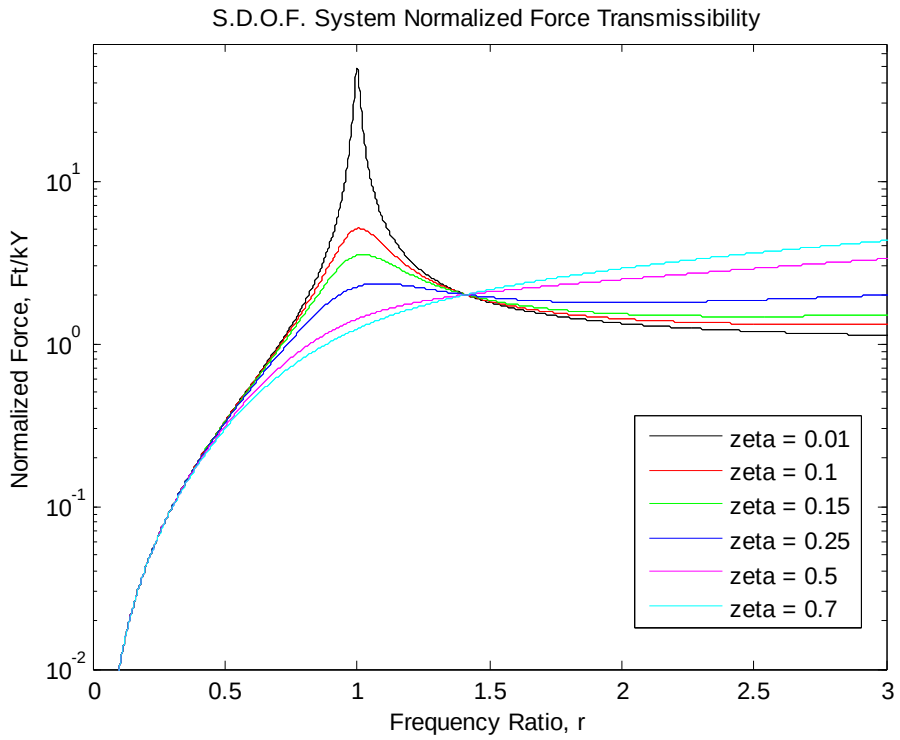

Figure 2.4 Force Transmissibility as a function of frequency for various ζ values

Considering again the one wheel bump input with excitation frequency $\omega_{bump} > \sqrt{2}$, Figure 2.4 demonstrates how drastically the force increases at higher frequency ratios. The same ζ value that reduces force transmitted to the sprung mass near resonance, now dramatically amplifies the force at higher frequency inputs.

Thus for a 'soft' ride, lower ζ values are preferred in order to minimize the forces experienced by the chassis. Low ζ values however, cause an increase in the amplitude of chassis motion and prevent the vehicle from settling into steady state behavior. This makes the vehicle respond sluggishly to driver inputs and experience overshoot in gross body motions. Figure 2.4 illustrates the compromise associated with passive suspensions.

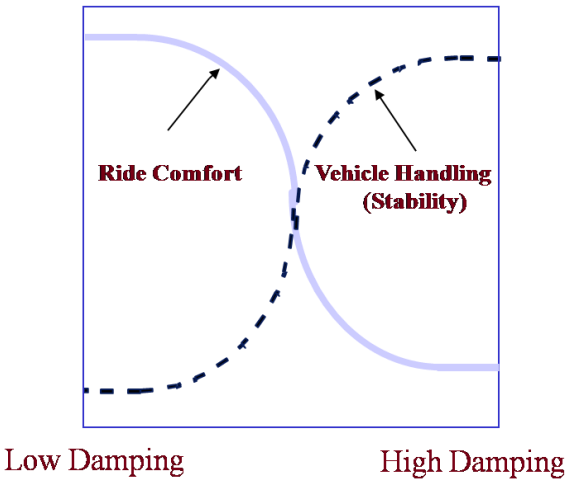

Figure 2.5 Ride vs. handling compromise associated with passive damping

2.3.2 Semi-active Dampers

Semi-active dampers allow electronic modulation of suspension damping forces according to a control policy. The distinction between active and semi-active suspensions is that the latter are not capable of generating any actuation force, but are only capable of controlling the amount of energy absorbed. Semi-active devices offer an attractive solution to eliminate the ride versus handling compromise associated with passive dampers, without the larger power consumption requirements from an active system.

A variety of semi-active damping systems exist, perhaps the most popular of which is magnetorheological dampers. In addition to MR dampers, electro-hydraulic solutions have also been developed and investigated. These dampers are usually composed of a voice coil (solenoid) actuated hydraulic proportioning valve mounted externally such that fluid flows through the valve in one direction, independent of the direction of damper velocity. Other types of electro-hydraulic dampers have certainly been studied, although their designs are typically proprietary. Magnetic dampers and eddy current dampers have been used in exercise machines and other low force applications, rarely in vehicles. The following literature review briefly covers an introduction to MR technology, MR dampers in heavy truck suspensions, as well as some existing electro-hydraulic dampers.

2.4 Literature Review

2.4.1 MR Dampers

MR dampers utilize magnetorheological fluids, instead of hydraulic oils, as the working fluid. The apparent viscosity of the MR fluid is varied by controlling the current through an electromagnet. This electromagnet creates magnetic flux path between the piston and damper body which locally energizes the fluid flowing through an annular gap between the outside of the piston and the damper body. A schematic of the flux path, piston, and damper body layout is shown in Figure 2.6, as well as a plot of the pressure drop and flow rate relationship for different magnetic field strengths [6].

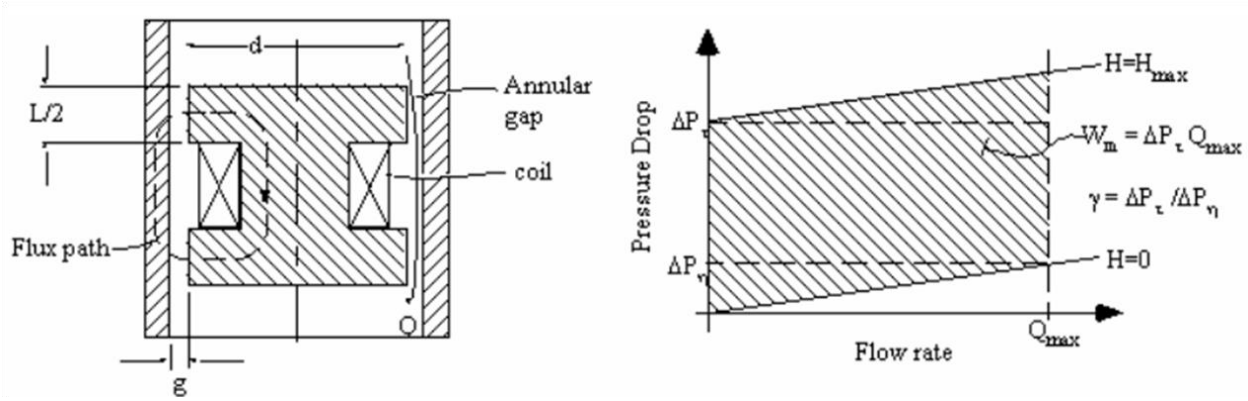

Figure 2.6 Section View: Typical mono tube MR damper **[**adapted from 6]

For a thorough treatment of MR fluid mechanics and MR damper design and characterization see Poyner [5]. A typical mono tube MR damper is shown in Figure 2.7 with a breakout section view of the piston assembly.

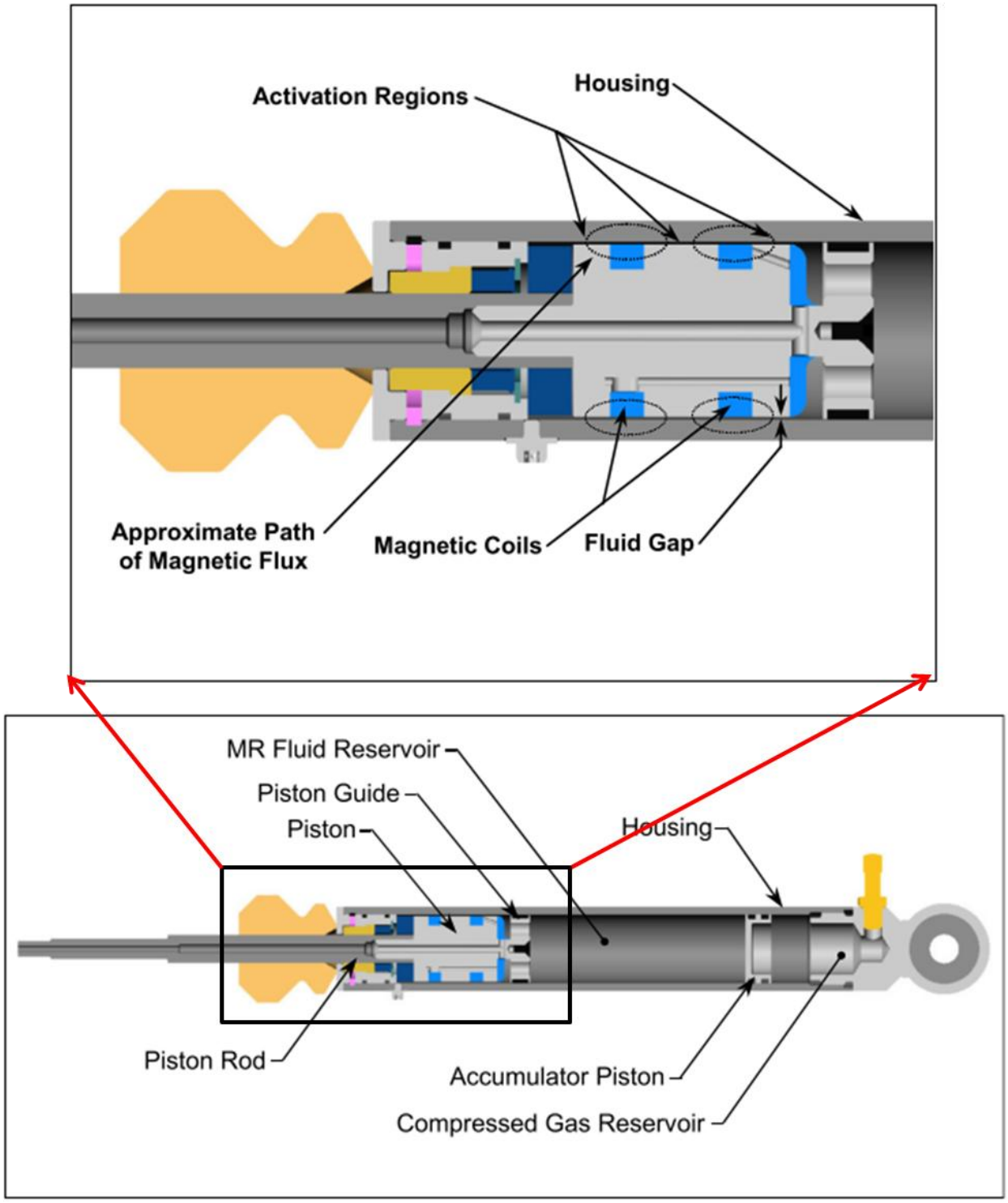

Figure 2.7 Section View: Typical mono tube MR damper **[**adapted from 5]

A great deal of research has been conducted on MR fluid behavior, device design, and commercial applications since the development of MR fluid by Jacob Rabinow at the U.S.

National Bureau of Standards in the late 1940's [7]. Jolly, et al. [7], discusses the research history of MR fluids and commercial applications. The Bingham Plastic model is covered as well as different flow modes and common device geometries. Lastly, properties of existing commercial fluids are discussed as well as a small linear MR damper and seismic MR damper designs. This paper illustrates the variety of properties attainable with different types of MR fluid and the engineering and design implications of these properties.

Ahmadian and Simon evaluate the performance of independently developed MR dampers installed on a Volvo Series VN heavy truck [10]. The test vehicle was instrumented with an array of accelerometers and each damper was controlled by real-time imbedded controller employing an on-off skyhook control policy. The controller utilized sprung mass and axle velocity measurements, obtained by integrating and filtering accelerometer data. Transient and steady state tests were performed and the resulting data was analyzed in the time and frequency domains for four distinct acceleration bandwidths. These bandwidths correspond to different vibration modes associated with heavy trucks like the test vehicle. The study demonstrated the ability of controllable dampers to change the average RMS and peak acceleration values experienced by the driver. This study further discusses some of the trade-offs of the test dampers on peak accelerations and settling time.

Mcmanus and St. Clair studied the shock attenuation performance of a commercially available MR damper system designed by Lord Corporation [14]. The operating principles of the damper are discussed and force velocity curves are generated through testing at multiple input currents. The damping system is tested in a truck seat suspension and transmissibility characteristics are determined. The MR damper was found to be most effective in situations where the OEM passive damper would have resulted in contact with the end stops.

Dogruer and Gordaninejad developed a MR damper for a high-mobility multi-purpose wheeled vehicle (HMMWV) [15, 16]. The test dampers were designed to outperform the OEM damper while maintaining the same geometric parameters. Additional design work was performed to ensure the damper performed as a failsafe damper, retaining a nominal level of asymmetric damping through the use of shims

Sahin, et al. developed a high force MR fluid bypass damper and corresponding empirical model [8]. Heavy vehicle roll stability is examined for two different control strategies, and compared with the uncontrolled MR damper and the OEM passive damper. The vehicle roll angle is examined during a transient emergency lane change maneuver. Simulation results show significant reduction in roll angle throughout the duration of the lane change maneuver.

Gordaninejad and Breese examined the effects of temperature on the force characteristics of three separate MR dampers [9]. Additionally, heat generation over time was evaluated experimentally. A theoretical model was developed to represent the temperature increase in a MR damper due to a constant sinusoidal input and current to the electromagnet. Selected results of this study will be discussed in further detail in Chapter 6 of this document.

2.4.2 Mechanically Adjustable Dampers

A significant amount of research has been conducted on electro-mechanically adjustable dampers, although much of it has been proprietary. Kitching, et al., developed a solenoid actuated spool valve hydraulic damper [12]. The non-linearity of the valve was modeled and evaluated experimentally through hardware in the loop testing. The semi-active damper showed the most influence in the low frequency bounce (heave) mode, reducing RMS body accelerations by up to 12.3 %, depending on road conditions. The semi-active damper was also shown to reduce peak absolute body acceleration due to transient bump inputs, without compromising settling time. The damper developed in [12] is similar to many other semi-active hydraulic dampers previously studied. ZF Sachs GmbH utilize a similar solenoid actuated proportioning valve in their Continuous Damping Control® semi-active hydraulic damping system.

Usman and Parker developed a low cost electro-hydraulic proportioning valve suitable for semi-active suspensions. Their goal was to reduce the unit costs associated with high precision machining, while providing a valve that is insensitive to fluid contamination and periods of inactivity [21]. A floating double disc configuration was developed and modeled mathematically. Magnetic and fluid forces versus displacement were calculated and used to relate differential coil current to disc position. Sun and Parker expanded on the previous work by integrating the double disc valve configuration into a semi-active damper [20]. Operating

principles are discussed and a theoretical model was developed. A PID controller was designed and the closed loop transfer functions are analyzed in Matlab. A prototype valve was tested and pressure versus flowrate characteristics determined. The dynamic tests on the valve showed that it is capable of meeting a bandwidth requirement of 50 Hz.

Other semi-active systems exist, outside the realm of solenoid actuated dampers. One such solution developed and patented by Wolfe, et al. [13] employs an external actuator to rotate a concentric bypass valve. This valve was developed for use in adaptive and semi-active systems with the goal of reducing actuator requirements through minimization of parasitic friction, pressure balancing, and inertia reduction. The valve developed in this study has a similar configuration, which will be explained in further detail in Chapters 3 through 5.

Chapter 3

Initial Prototype Mechanically Adjustable Hydraulic Damper Design, Fabrication, and Characterization

Two prototype dampers were prototyped and tested throughout the course of this research. These dampers were tested extensively and redesigned through multiple iterations. This chapter is concerned with the development of the Initial Prototype mechanically adjustable hydraulic damper. This damper initially served as a proof of concept prototype and then was refined to exhibit more desirable force characteristics. After a brief introduction to hydraulic damper mechanics, this chapter will cover the design of the Initial Prototype damper, fabrication, including select technical drawings, as well as its force characterization.

3.1 Hydraulic Damper Operating Principles

Conventional hydraulic dampers work by passing fluid through an orifice, or series of orifices, in response to the presence of a displacement input. When the working fluid, typically petroleum based oil, is passed through the damper valves, a pressure differential is created on opposing sides of the piston. This pressure differential acts upon the area of the piston to create a force which opposes damper motion. To better understand the nature of the various forces at work in a conventional monotube damper, a free body diagram (FBD) is shown in Figure 3.1.

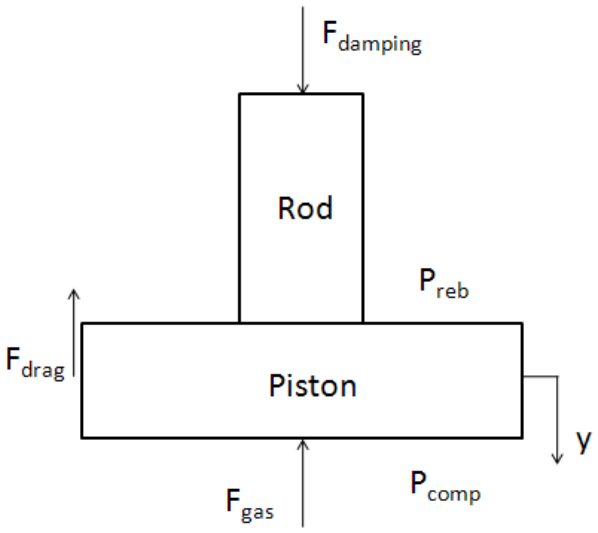

Figure 3.1 Free body diagram of damper internals

In addition to the damping, drag, and gas forces shown in the FBD, the pressures on the rebound and compression sides (P_{reb} and P_{comp}, respectively) give rise to the dominant force which reacts $F_{damping}$. A force balance in the y-direction yields,

$$\begin{aligned} &\sum F_y = 0 \\ &F_{damping} + P_r\left(A_p - A_r\right) - P_c\left(A_p\right) - F_{drag} - F_{gas} = ma_y \end{aligned} \tag{3-1}$$

where $F_{damping}$ is the input force, P_{reb} and P_{comp} are the static pressures on the rebound and compression sides of the piston, A_p is the area of the piston, A_r is the cross sectional area of the rod, F_{drag} is the coulomb friction force between piston guide and damper body, and F_{gas} is the force due to the gas reservoir. F_{drag} is a function of the materials used for the wear band, damper body, damper rod, and main bearing, their surface finishes, and the fitment between them. For this analysis F_{drag} is neglected because it is generally very small when compared to fluid forces. F_{gas}, which depends on the pressure in the gas reservoir and the rod area upon which this pressure acts, is also neglected because it gives rise to a spring force that is independent of velocity. The mass m in (3-1) is relatively small and thus its acceleration may be neglected for this simple analysis. By rewriting equation (3-1) and neglecting non-dominant forces equation (3-2) is obtained.

$$F_{damping} + P_{reb}\left(A_p - A_r\right) - P_{comp}\left(A_p\right) - \cancel{F_{drag}} - \cancel{F_{gas}} = \cancel{ma_y}$$
$$F_{damping} = P_{comp}\left(A_p\right) - P_{reb}\left(A_p - A_r\right) \tag{3-2}$$

Thus one can easily see that the damping force depends largely upon the pressure differential between opposing sides of the piston. Understanding the nature of this pressure difference and the fluid dynamics occurring at the piston is crucial for both the passive and semi-active damper designer. It is especially important for the semi-active damper design because valve geometry may be manipulated in real time as a means of controlling main piston pressure differential.

The pressure differential across the piston in a conventional passive damper is a function of the piston geometry and the stiffness of the shims stacked on either side. Damper designers use different stacks of shims to achieve the desired stiffness for the separate rebound and compression check valving. When fluid passes through the main piston orifices, the shims deflect according to the velocity (dynamic pressure) of the fluid passing by them. Thus the effective area of the valve is constantly changing as input velocity changes. Careful control of this effective area allows damper designers and builders to achieve the force velocity characteristics that best suit the mechanical system they are trying to attenuate. The effective area can be reasonably approximated if we know the tip deflection and the radius of the largest shim, as shown below in Figure 3.2.

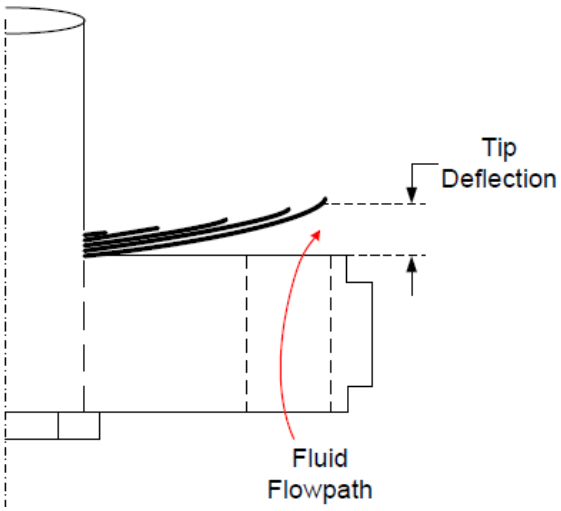

Figure 3.2 Half section view of a passive damper showing flow path and shim deflection

Examining effective area due to tip deflection provides insight into total orifice area requirements needed in subsequent prototype orifice-control dampers.

3.2 Initial Prototype Design

The Initial Prototype mechanically adjustable damper is a monotube design with a main piston, a base valve and no external valving. A section view of the damper is shown below in Figure 3.3 (base valve excluded).

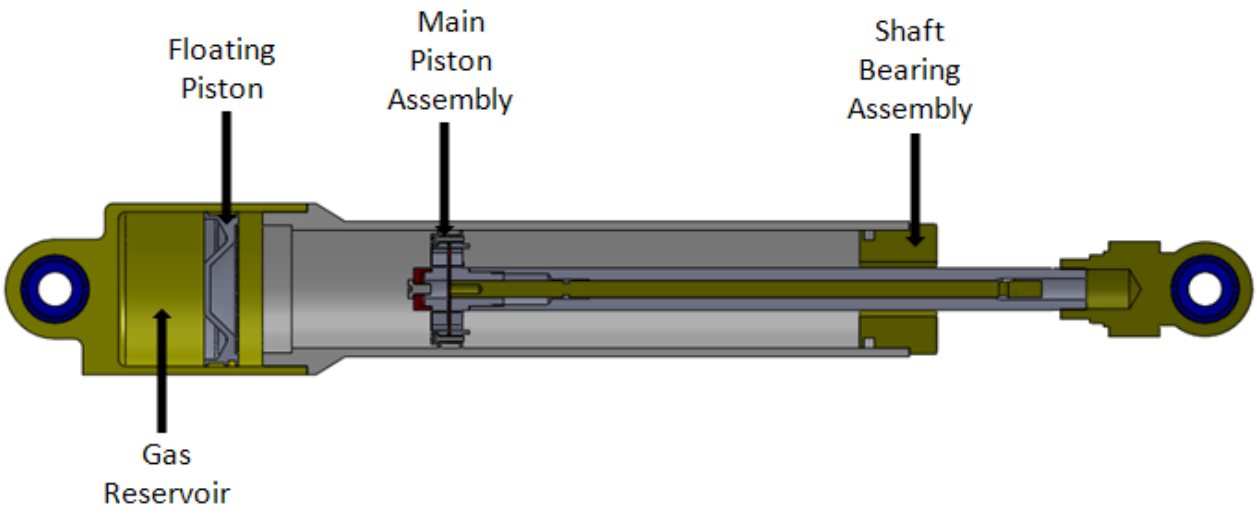

Figure 3.3 Initial Prototype damper section view with base valve removed

Similar to passive dampers, the Initial Prototype damper utilizes shims as check valves that control the directionality of the flow through the piston orifices. Unlike passive dampers, the shims on the Initial Prototype damper are not used to provide the majority of the flow constriction and damping force. Instead, a disc valve is incorporated within a two piece piston. The orifices on the disc can be rotated out of phase with the orifices on the main piston, allowing the effective flow area of the valve to be controlled via external actuation. The valve design is shown in further detail in Figures 3.4 and 3.5, each depicting section views of the piston assembly, the first of which includes the control rod that rotates the internal disc.

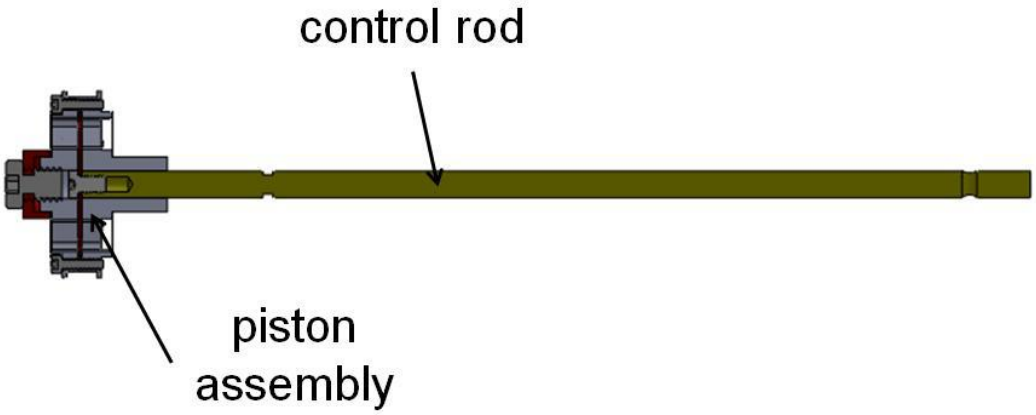

Figure 3.4 Section view of main piston assembly and disc valve control rod

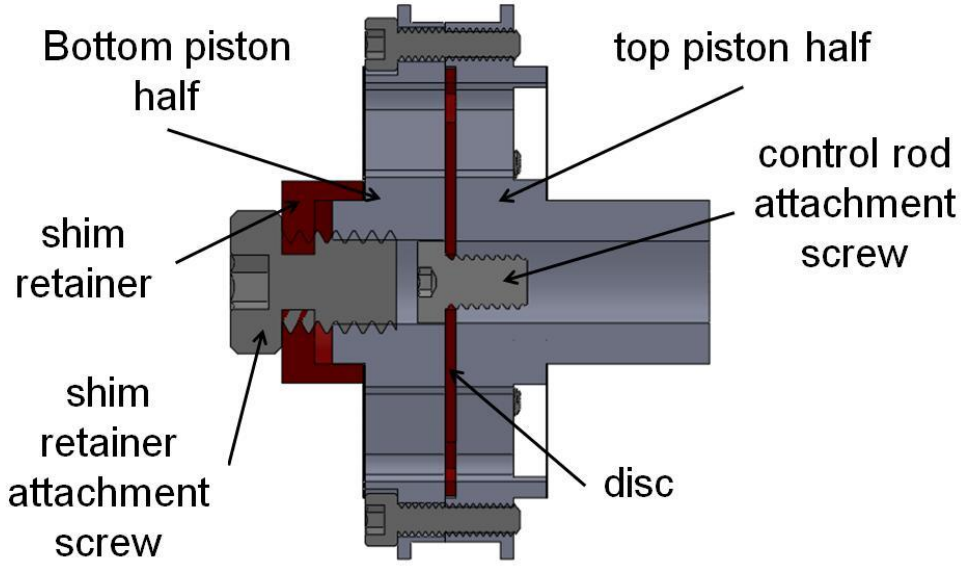

Figure 3.5 Section view of main piston assembly, excluding disc valve control rod

Because thin shims are used on both sides of the piston, their compliance prevents them from causing a large pressure drop and corresponding damping force. The purpose of using thin shims is to decouple the rebound and compression valving. For an integral disc with six orifices, rebound and compression each have three dedicated orifices per disc, as illustrated in Figure 3.6.

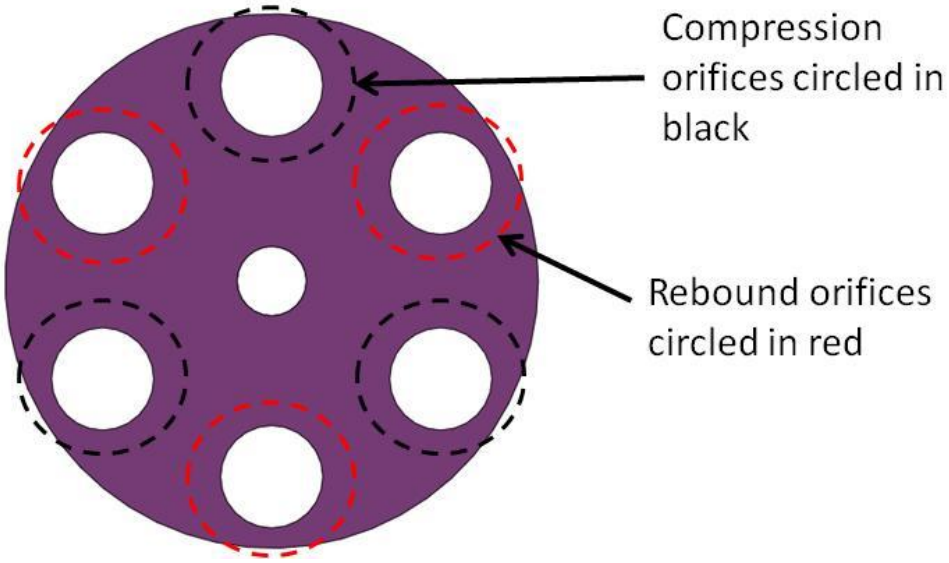

Figure 3.6 Example of decoupled disc valve geometry

The rebound and compression decoupling is important because desired rebound and compression damping often differ considerably.

3.3 First Iteration Disc Valve Design

The first piston assembly design consisted of a radial array of six equally sized holes, providing symmetric rebound and compression orifice area. The disc incorporated an identical array of holes, such that when turned in phase with the piston orifices the fluid path remained completely unblocked.

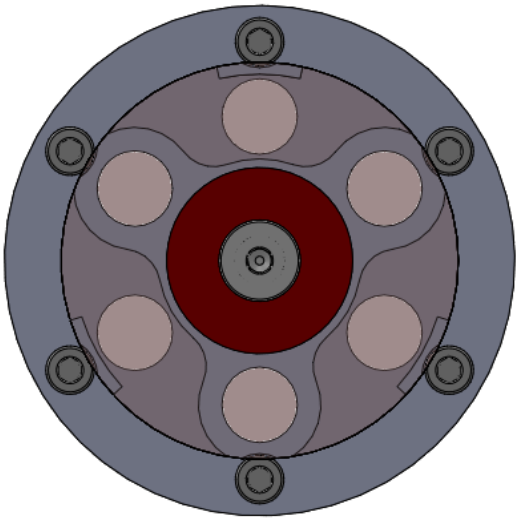

Figure 3.7 First iteration valve design

This design was intended to be an initial test piece, used primarily as a proof of concept and a means for understanding how damping force changes with orifice area.

Since changing the disc position is the primary method of controlling damping characteristics, understanding the disc position and damping force relationship is of vital importance. Let us first consider the flow through our piston as pipe flow. Assume a shock velocity of 3 inches per second, which corresponds to gross body motion in vehicles with ride and roll frequencies around 1 Hz. This shock velocity will give rise to a fluid velocity in our idealized pipe according to the following equation.

$$u_{fluid} = \left(\frac{A_{piston}}{A_{orifice}}\right)V_{shock} = \left(\frac{D_{piston}^2}{3D_{orifice}^2}\right)V_{shock}$$
$$u_{fluid} = \left(\frac{1.72^2}{3\times(0.25^2)}\right)\times 3\text{inch/s}\times\left(\frac{1\text{ft}}{12\text{inch}}\right) = 3.94\text{ft/sec} \quad (3\text{-}3)$$

Assuming typical SAE 30 oil properties, the Reynolds number for our idealized pipe flow is calculated to be

$$\text{Re} = \frac{\rho u D}{\mu} = \frac{\left(912kg/m^3\right)\left(3.94\text{ft/sec}\right)\left(.3048m/\ ft\right)\left(0.25in\right)\left(\frac{1\,ft}{12in}\right)}{3.8\times10^{-1}N\times s/m^2} \quad (3\text{-}4)$$
$$\text{Re} = 60.045$$

For such low Reynolds number flow, a low friction factor is expected. Coupled with the short effective pipe length of the piston, we can neglect the pressure drop associated with the frictional interaction between the oil and the piston walls. Therefore it is safe to assume that the dominant pressure loss is a result of viscous dissipation and dynamic pressure recovery. By neglecting surface friction, we can now focus solely on how the disc position affects dynamic pressure, and ultimately the damping force.

A good way to gain some insight into the relationship between disc position and damping force is to first look at the disc position and orifice area relationship. A plot of valve area vs. disc rotation for the first iteration valve design is shown below in Figure 3.8.

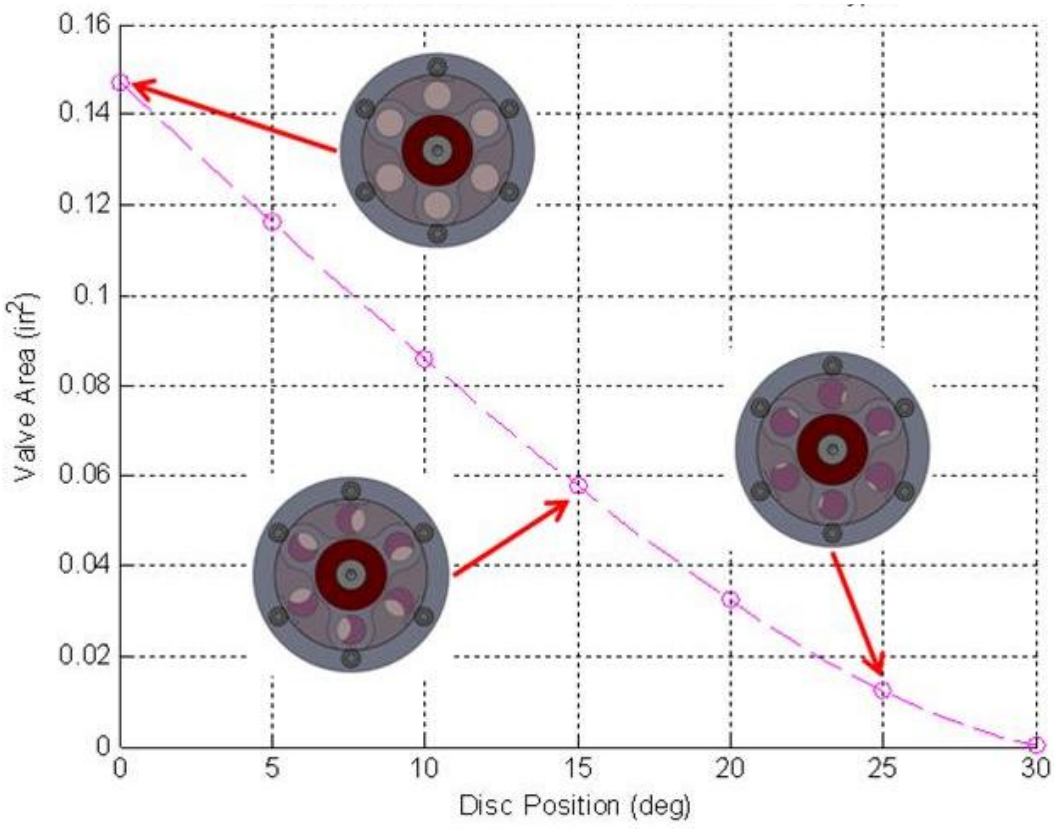

Figure 3.8 First iteration orifice area and disc position relationship

As expected, the change in valve area is non-linear with change in disc position. The first iteration valve design was used primarily as a proof of concept. Consequently, packaging was the primary design concern, as opposed to individual orifice geometry.

Using Bernoulli's equation, the following correlation between pressure drop and fluid velocity is determined,

$$\Delta P = Kq = K\frac{1}{2}\rho u^2 \tag{3-5}$$

where K is a loss coefficient and u is fluid velocity. From this relationship, approximately how the damping force changes with valve area, and thus disc position, can be determined. This relationship and the test results allow us to design subsequent valve geometry which yields more desirable damping characteristics.

3.4 Experimental Setup and Test Results

Initial tests were performed on a Roehrig EMA shock dynamometer with a 2500 lbf load cell. The experimental setup is shown below. The valve position was adjusted manually and locked via an external screw guide.

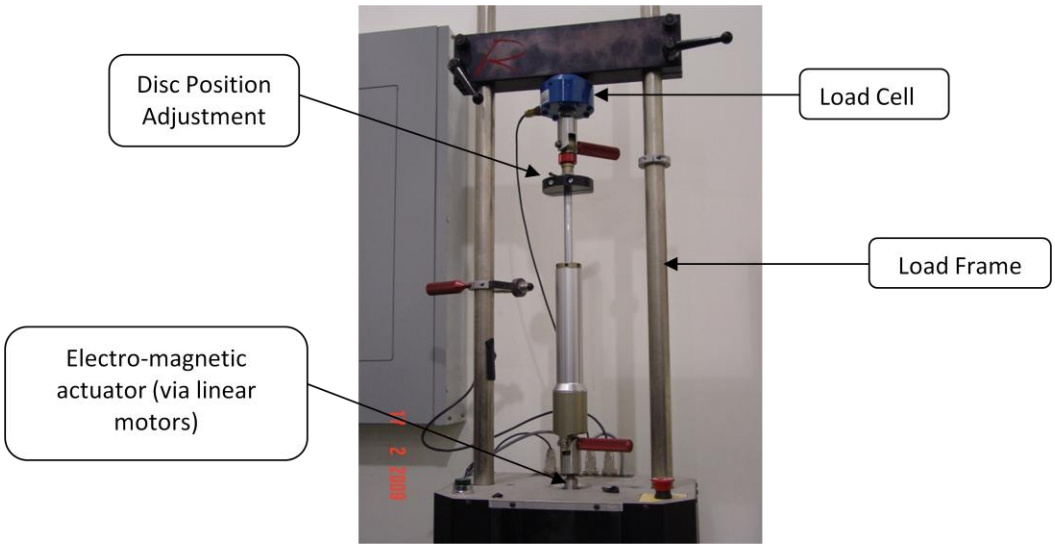

Figure 3.9 Experimental setup for first iteration tests

Initial test results show the damper is capable of generating a large force range. For a 2 Hz, 2 inch peak-to-peak sinusoidal input the compression adjustment is 20:1 while the rebound adjustment is 12:1. A plot of these test results is shown in Figure 3.10.

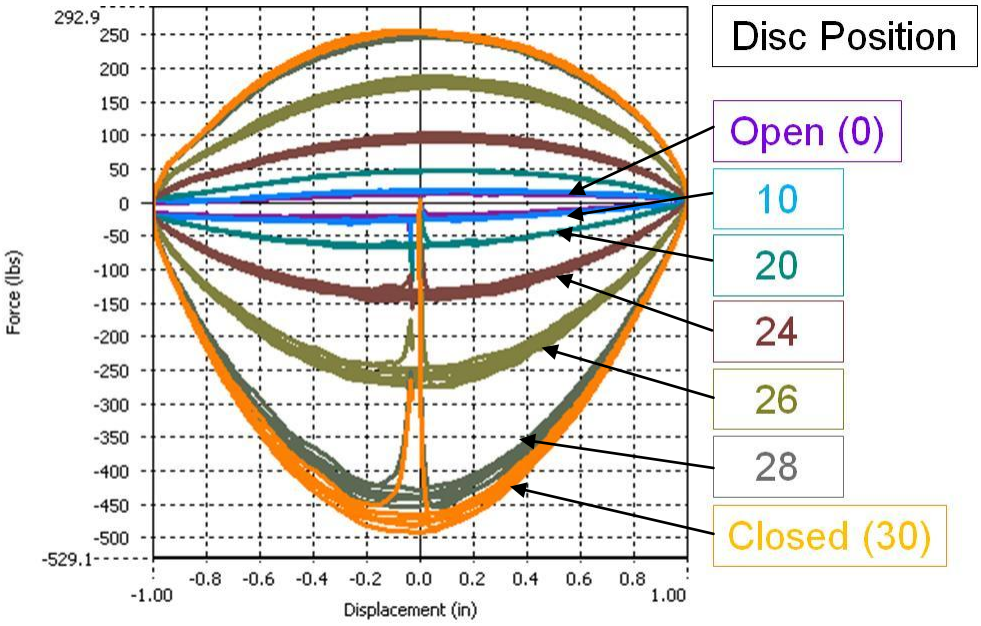

Figure 3.10 +/- 1 inch @ 2 Hz sinusoidal input, Force vs. velocity plot

To better understand the damping force vs. disc position relationship, peak forces associated with each discrete valve setting for the 2 Hz test shown in Figure 3.10 are plotted in Figure 3.11.

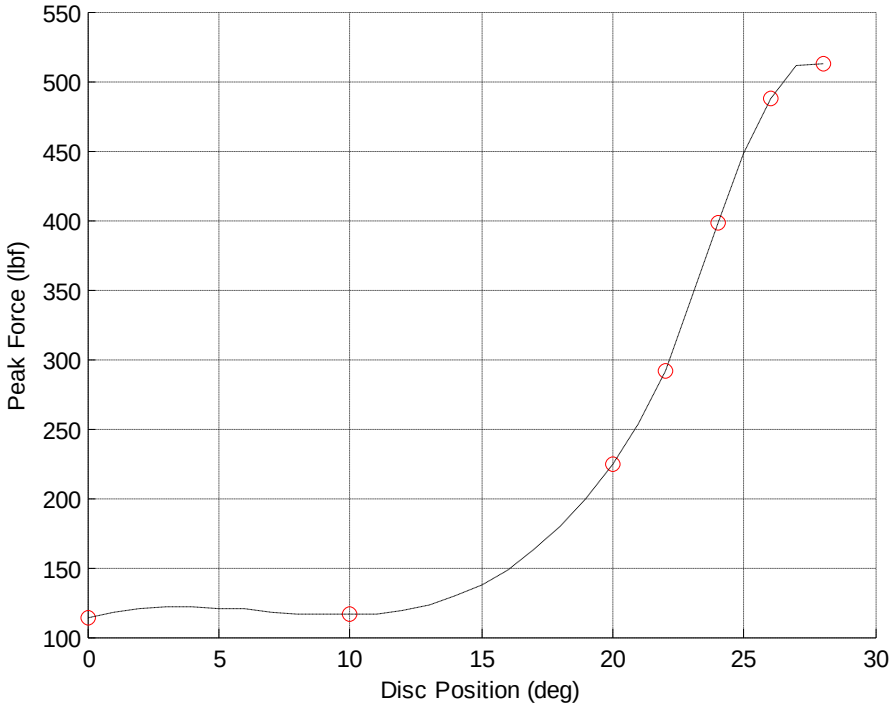

Figure 3.11 Peak force of the second iteration design as a function of disc position, for +/- 1 inch peak displacement at 2 Hz sinusoidal input

Figure 3.11 explicitly shows the non-linear relationship between disc position and damping force. It is worth noting that the peak force is most sensitive to change between approximately 15 and 30 degrees of disc rotation. This shows that almost half of the adjustment range is ineffective. For a peak force F and a disc rotation angle θ, sensitivity can be defined using ,

$$\frac{\partial^2 F}{\partial \theta^2} = sensitivity \tag{3-6}$$

To minimize this sensitivity, the desired valve characteristics can represented by,

$$\frac{\partial^2 F}{\partial \theta^2} = 0 \tag{3-7}$$

$$\frac{\partial F}{\partial \theta} = c \tag{3-8}$$

Thus for an identical range of peak force as obtained in the experimental results shown in Figure 3.11, the desired peak force vs. disc position relationship is shown by a straight line on Figure 3.12.

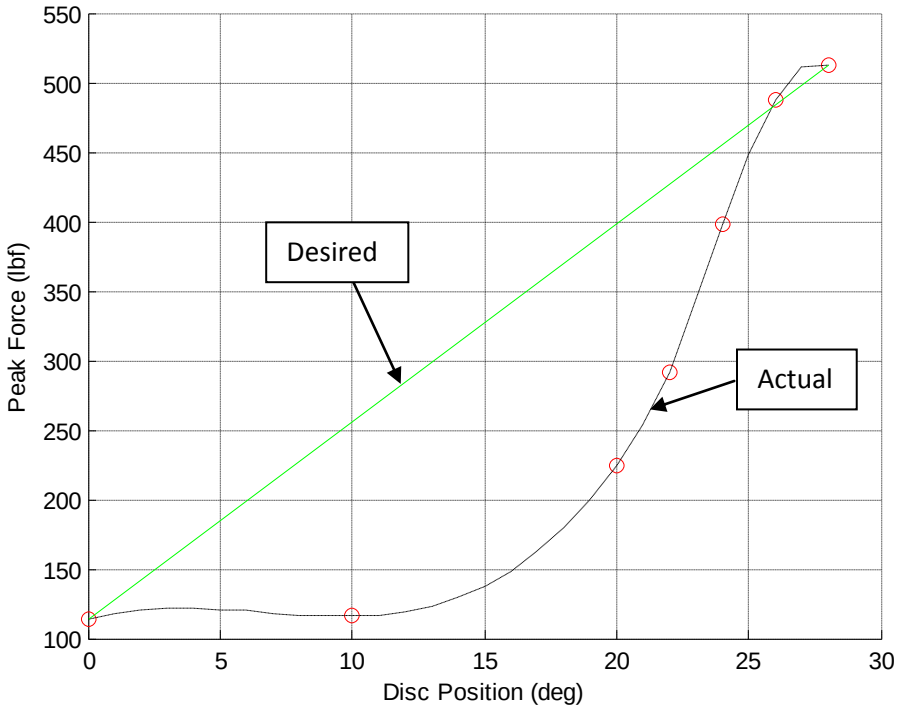

Figure 3.12 Desired force and first iteration comparison plot. Peak force as a function of disc position, for +/- 1 inch peak displacement at 2 Hz sinusoidal input

Now that the desired valve sensitivity is defined, the practical reasons for minimizing sensitivity must be identified, before discussing the subsequent design iterations performed to meet performance goals. A control scheme using a simple lookup table describing force vs. disc position could be employed to work around the nonlinear sensitivity of the valve, but there are other practical reasons for minimizing valve sensitivity.

Minimizing sensitivity reduces the requirements for the actuator to correctly select the disc position. Stepper motors, for instance, are only capable of moving in discrete steps. These steps are a function of the motor's designed step resolution. If the valve design is less sensitive to position changes, then a less precise actuator is required, thus a stepping motor with a larger resolution can be employed. Reduced valve sensitivity limits the effects of position error to the lowest achievable level for a given force range. Along the same lines, minimizing sensitivity reduces undesired changes in damping due to any rotational compliance $\partial\theta$ in the system. It also ensures that compliance effects will be consistent regardless of absolute disc position θ. Reduced sensitivity also translates into larger allowable manufacturing tolerances and lower machining costs. Lastly, minimizing valve sensitivity allows for more accurate prediction of damping ratio as a function of measured position. This enables more robust and inexpensive control by minimizing the performance cost associated with measurement errors in a feedback control loop.

3.5 Design Issues and Redesign

From fluid dynamics and basic pipe flow, *major losses* are pressure losses due to friction between a fluid and the inner surface of the pipe. *Minor losses* are pressure losses due to geometry such as bends or other obstructions. In the case of a damper, the flow through the piston is nowhere near fully developed and the "pipe" length is so short that major losses are negligible. The primary sources of pressure losses are the entrance and exit geometry of the piston. As an example, sharp edged entrance geometry is shown below in Figure 3.13.

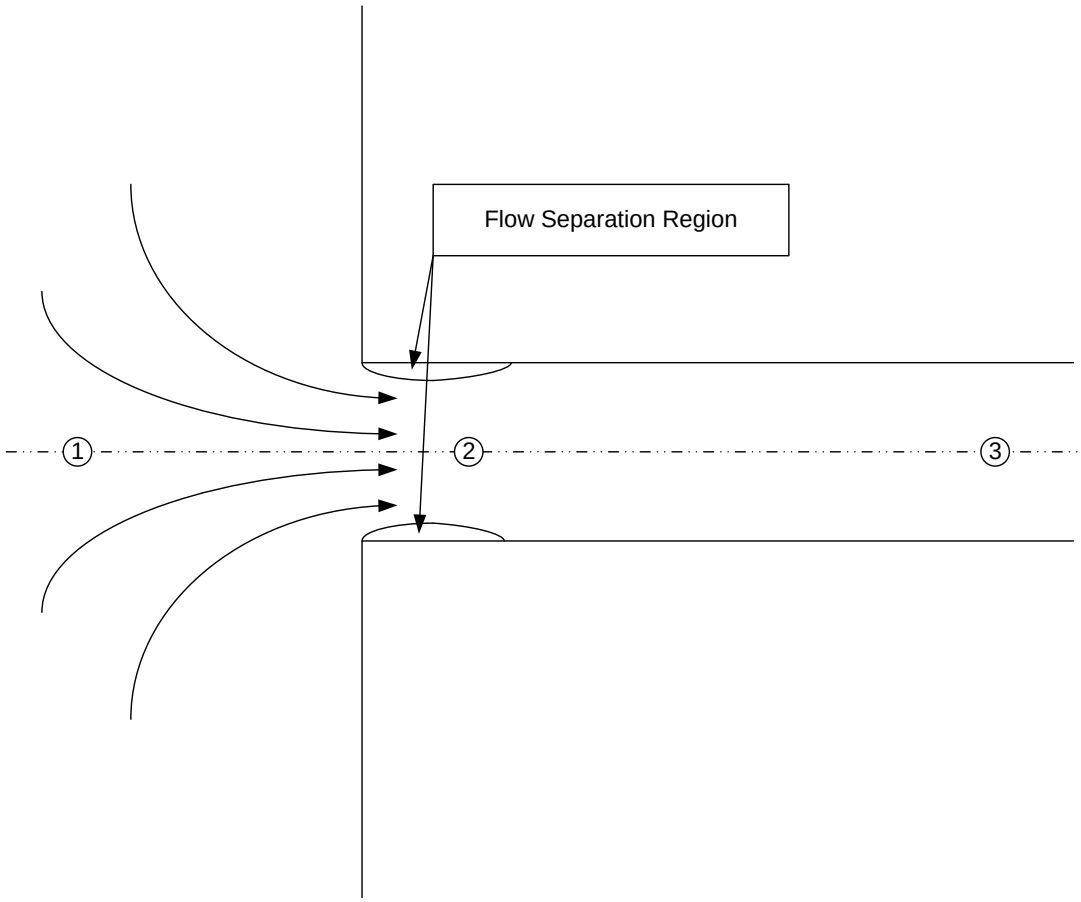

Figure 3.13 Entrance flow region of idealized pipe

Entrance pressure losses can be expressed mathematically through the use of a loss coefficient K_L. Consider point 3 in Figure 3.13 to be a point downstream where flow has become reattached to the pipe wall. At this point pressure recovery has occurred and much of the kinetic energy at point 2 has been converted to pressure. Because of the entrance geometry, some energy is lost through viscous dissipation, which can be expressed as head loss h_{loss} described in equation (3-9).

$$h_{loss} = K_L \frac{\rho V_3^2}{2} \tag{3-9}$$

The expression in (3-9) can be used to help develop more favorable disc geometry. The velocity of the flow through the piston at a given damper velocity is solely a function of orifice area. Thus, for a given damper velocity, there is a distinct disc geometry that minimizes valve

sensitivity. The goal of the second and third iterations of disc design is to determine this distinct disc geometry.

For a constant loss coefficient K_L, and constant oil density ρ, equation (3-9) clearly demonstrates that pressure loss, and by extension damping force, are solely a function of fluid velocity V. This idealized and rudimentary relationship serves as the starting point for our second iteration valve design. Fluid velocity in the piston is proportional to orifice area. Because damping force changes with the square of fluid velocity, it stands to reason that a disc designed with a quadratically changing orifice area (as a function of rotation angle θ) could be used to help linearize the change in damping vs. disc position. To investigate this theory, a new disc geometry was designed and tested.

First, the total area of the rebound and compression sides is defined in order to set the minimal or "off state" damping level. Based on packaging constraints, the total swept angle for each orifice is limited to 30 degrees. There is only one valve geometry that satisfies the total orifice area requirements for 30 degrees of available rotation, while ensuring this area changes as a second order polynomial through its available rotation. This unique valve geometry, used for the second iteration disc design, has an area vs. position relationship described by (3-10).

$$\text{valve area} = 7\times10^{-5}\theta^2 - 0.0052\theta + 0.1007 \qquad (3\text{-}10)$$

A plot of the valve area vs. disc position is shown in Figure 3.14. The second iteration valve design is displayed in red, overlaid on the first iteration valve design data from Figure 3.8.

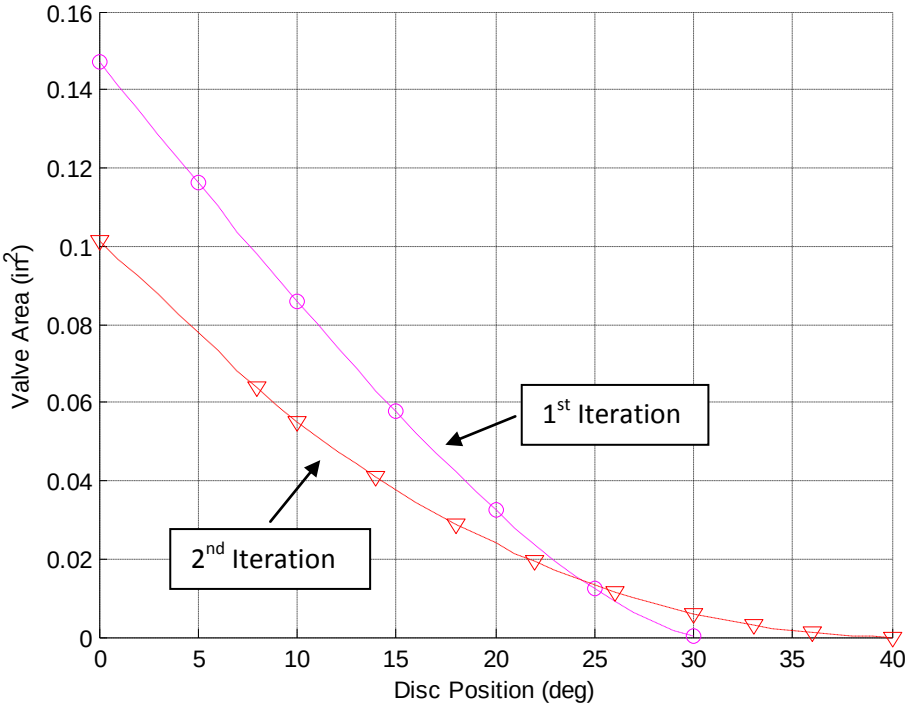

Figure 3.14 First and second iteration valve area vs. disc position comparison plot

A Solidworks rendering of the second iteration disc design is shown below in Figure 3.15, along with the modified piston assembly in Figure 3.16.

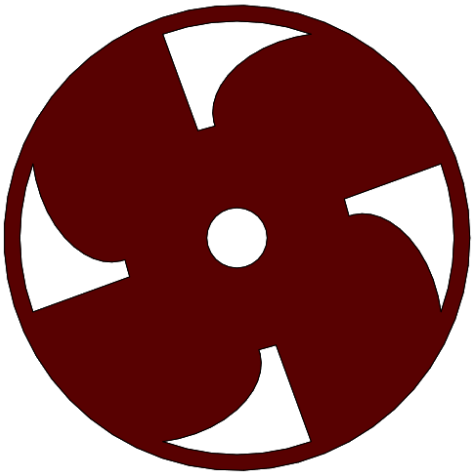

Figure 3.15 Second iteration disc design, front view

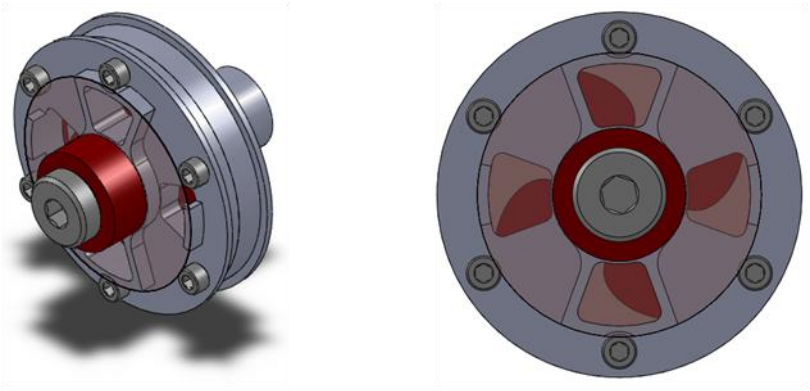

Figure 3.16 Second iteration piston design, isometric and front views (guide ring not shown in isometric view)

3.6 Second Iteration Test Results

Based solely on the plot in Figure 3.14, valve sensitivity is expected to decrease and the force vs. disc position relationship is expected to be more linear. This, however, is not reflected in the test results shown in Figure 3.17.

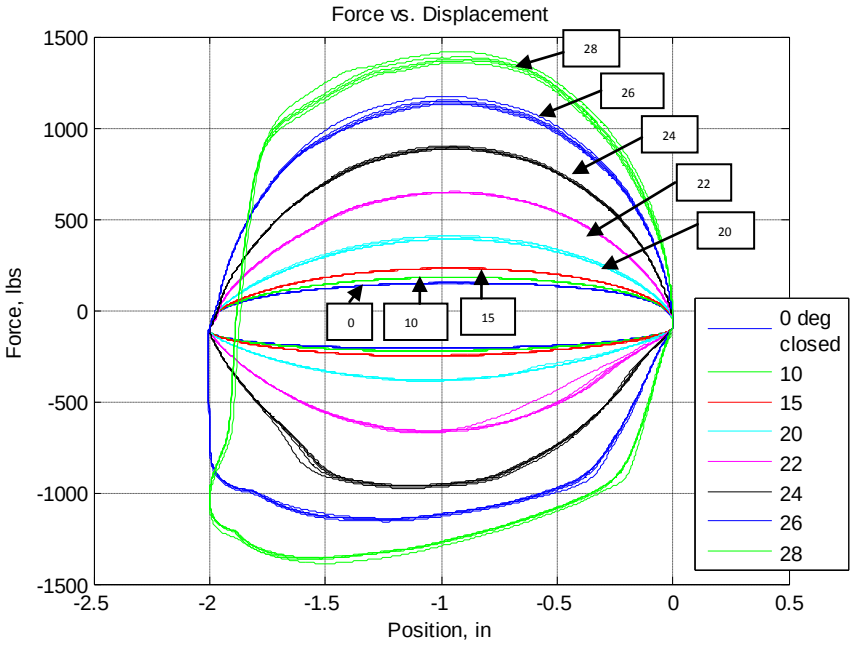

Figure 3.17 Second iteration test results for +/- 1 inch peak displacement, at 1 Hz sinusoidal input

When peak forces are plotted it is clear that the valve is still only sensitive to change above 20 degrees of valve closure.

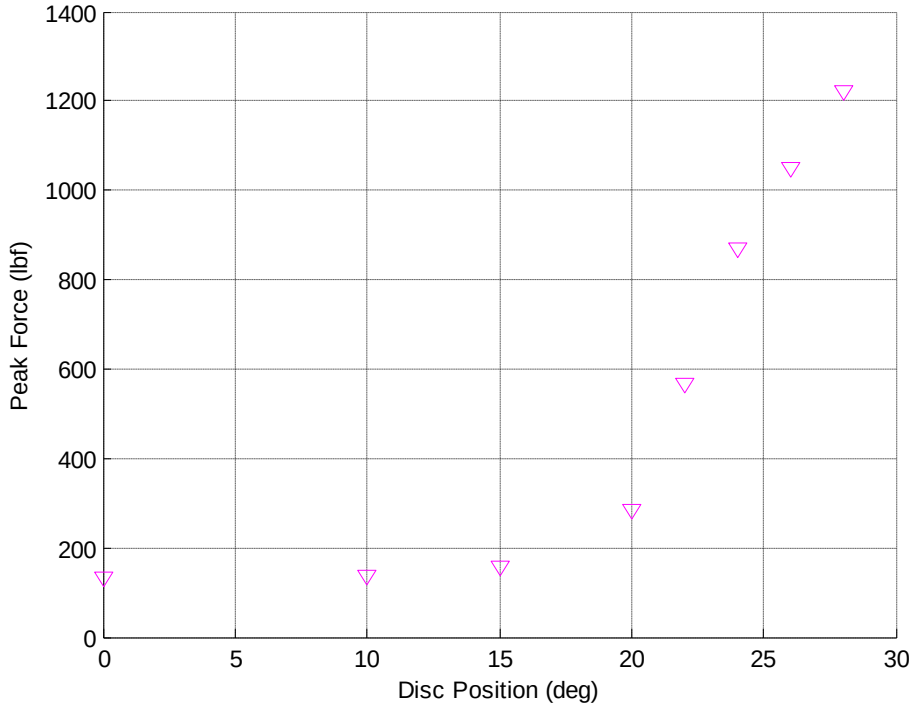

Figure 3.18 Peak force of the second iteration design as a function of disc position, for +/- 1 inch peak displacement at 1 Hz sinusoidal input

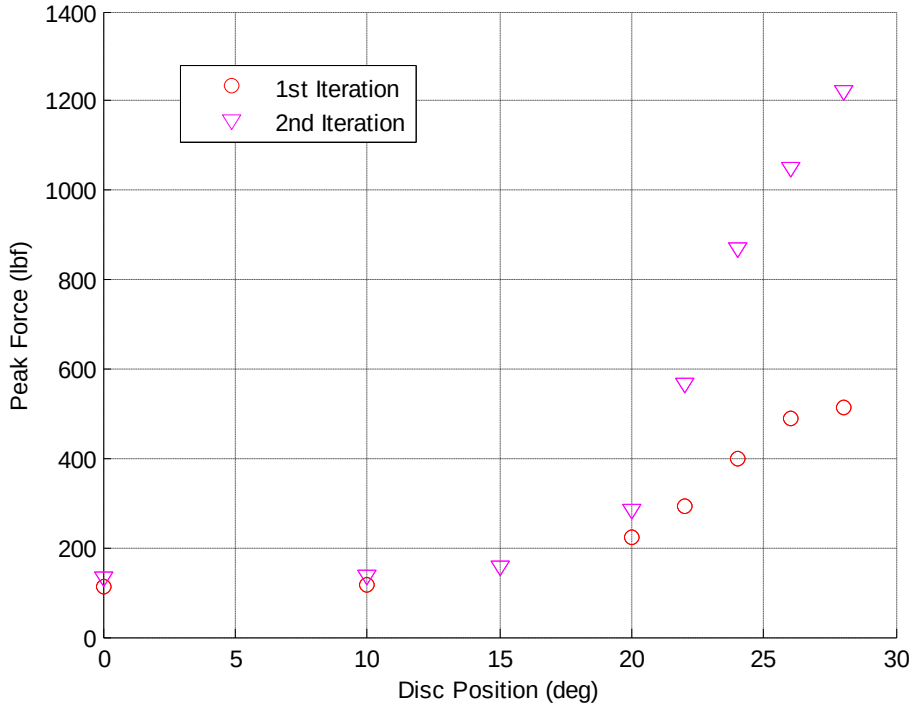

Figure 3.19 First and second iteration comparison of peak force vs. disc position

Although the valve remains sensitive, the second iteration design resulted in a much larger force range. The off state damping (fully open valve) resulted in 130 *lb* of peak force, while the 28 degree valve position resulted in 1221 *lb* of force. Additionally test results were not plotted because they caused further cavitation, resulting in no significant gains in peak force.

Due to the difference in peak forces and disc rotation range, it is difficult to compare the sensitivity of the first and second iteration valve designs. Normalizing based on peak force and disc position allows direct comparison of the two designs.

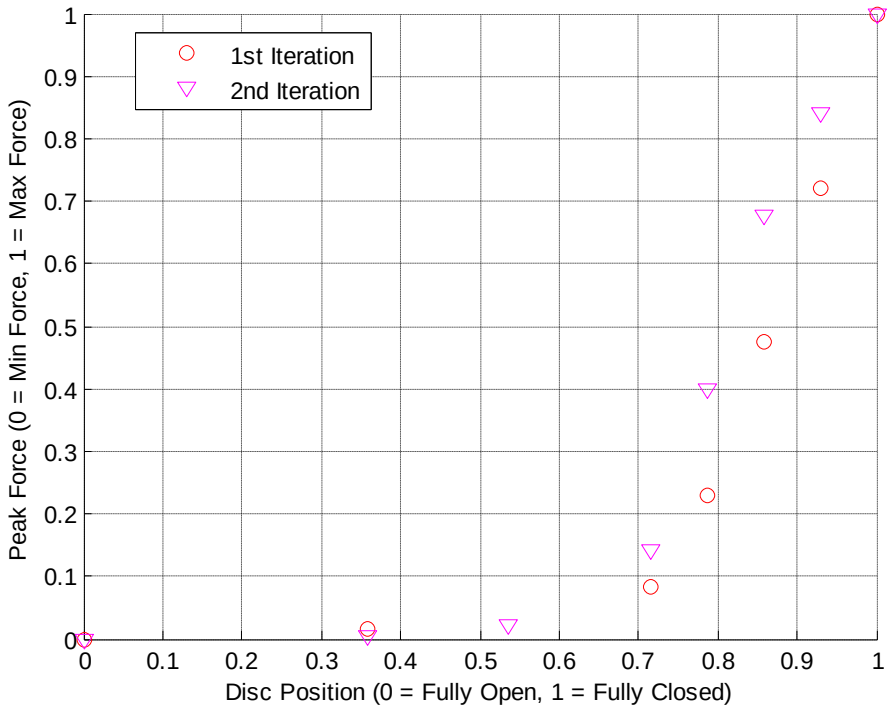

Figure 3.20 First and second iteration comparison of normalized peak force vs. normalized disc position

Figure 3.20 shows only a slight difference in valve sensitivity between the two iterations. The lack of change in valve sensitivity is unexpected. Between the first and second iterations, however, significant improvements in piston and disc fitment were made. These improvements in component fitment resulted in a reduction in leak paths, and are thus responsible for the significant increase in force seen in second iteration test results. Although the increase in peak force overshadows the effects of the new valve geometry, the second iteration disc is closer to our ideal design.

Another possible source of error is the changing nature of the minor losses associated with the disc geometry. As the disc is rotated in the housing, the inlet and outlet geometry change in addition to the valve area. This changing geometry results in a loss coefficient K_L which is not constant for all valve positions. CVeSS damper models have shown that loss coefficients, and associated minor losses, can have a dominant effect on damper force [11].

3.7 Notes on Fabrication

The piston halves were CNC machined from 6061 aluminum and the internal discs were originally Delrin with a thickness of 0.125 inches. Both piston halves were turned and milled manually. After first iteration testing revealed excessive forces tending to close the disc valve during operation, the Delrin discs were abandoned in favor of thin sheet stainless steel. The second iteration discs were laser cut and hand polished. Burrs were removed with a Dremil tool and the final surface finish was achieved through wet sanding with 1000 grit sandpaper. Sanding was performed by rubbing the disc itself on a sheet of 1000 grit paper taped to a smooth flat granite block. Though time intensive, this procedure yielded very low friction and resistance to movement in the final piston assembly. The control rod is AISI 1566 steel case hardened to a depth of 0.027 inches, with a surface finish of approximately 12 R_q and a straightness tolerance of 0.002 inches per foot. The guide rod seal is an o-ring made of buna, seated in a groove cut into the end of the control rod.

Chapter 4

Final Prototype Mechanically Adjustable Hydraulic Damper Design and Fabrication

This chapter is concerned with the development of the Final Prototype mechanically adjustable hydraulic damper. Coverage includes all aspects of the mechanical design of the full scale prototype, including some assembly level design drawings. All other design drawings of sub-assemblies and components can be found in the Appendix. The functionality of the components and the operating principals of the damper are discussed. Details on fabrication such as material choices and seal specifications are also included.

4.1 Final Prototype Damper Design

The Final Prototype mechanically adjustable damper is also a monotube damper with a main piston, no base valve and no external valving. A section view of the damper is shown below in Figure 4.1.

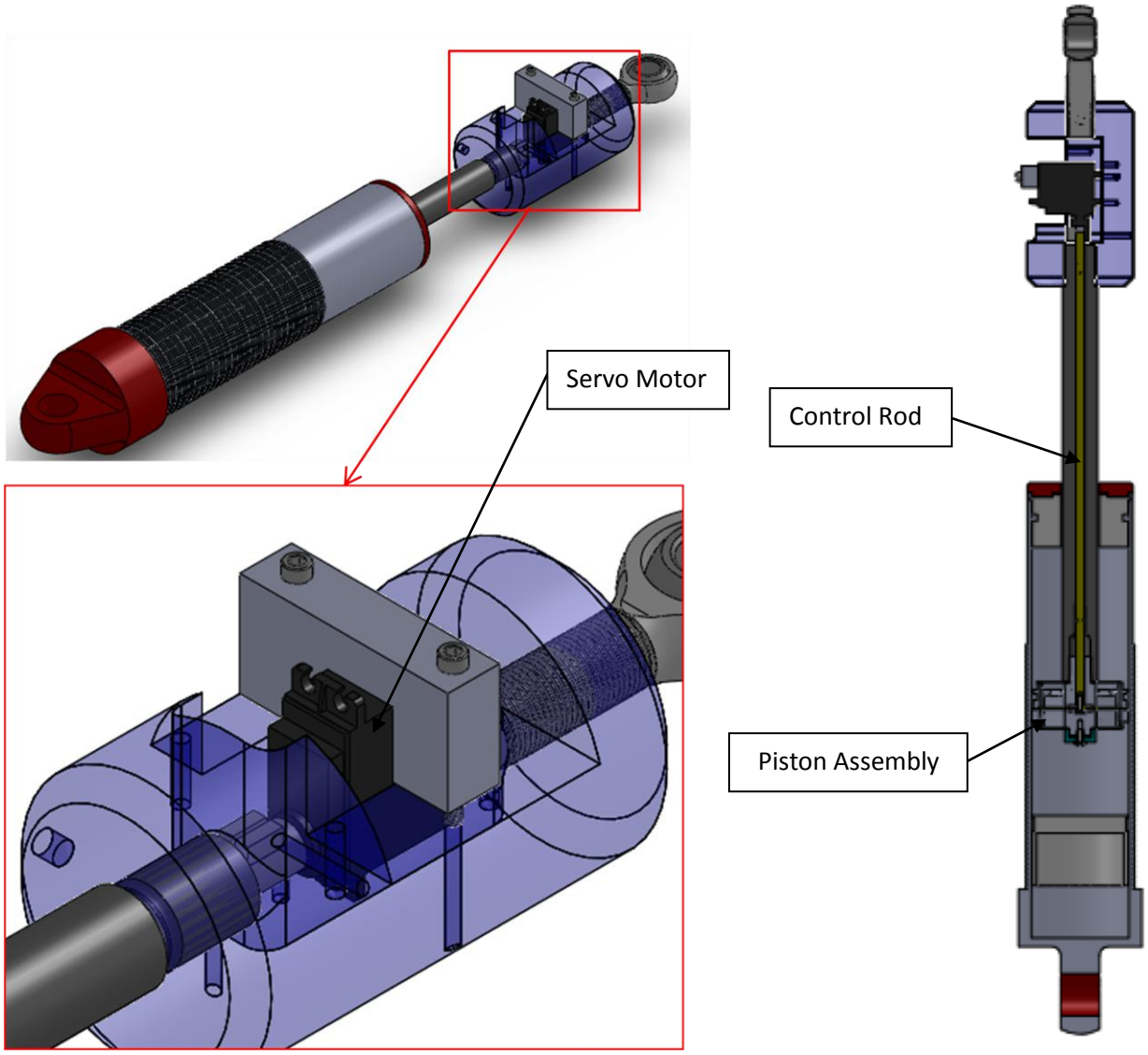

Figure 4.1 Final Prototype Damper, isometric, iso-close, and section views

The Final Prototype damper shares much of the same design architecture as the Initial Prototype, only scaled up to a level more appropriate for implementation in heavy truck applications. The shock bore is 2.77 inches and the stroke is approximately 7 inches, depending on the desired gas

chamber volume. The piston design remains largely unchanged in that it is composed of two halves encompassing a thin center disc. This disc is connected to a control rod which runs the length of the damper rod to a concentrically mounted servo motor. The servo motor is bolted in a housing which connects the damper rod and the spherical bearing at the top of the damper. This servo is designed to change the valve position in a real-time control application.

Though largely unchanged, there are some subtle differences in the piston designs of the Initial and Final Prototype dampers. Most of these design changes are driven by packaging and stress requirements; however, there is a difference in the inlet geometry. A large radius has been cut on the edge of the inlet ports. This radius is shown in the Solidworks rendering in Figure 4.2.

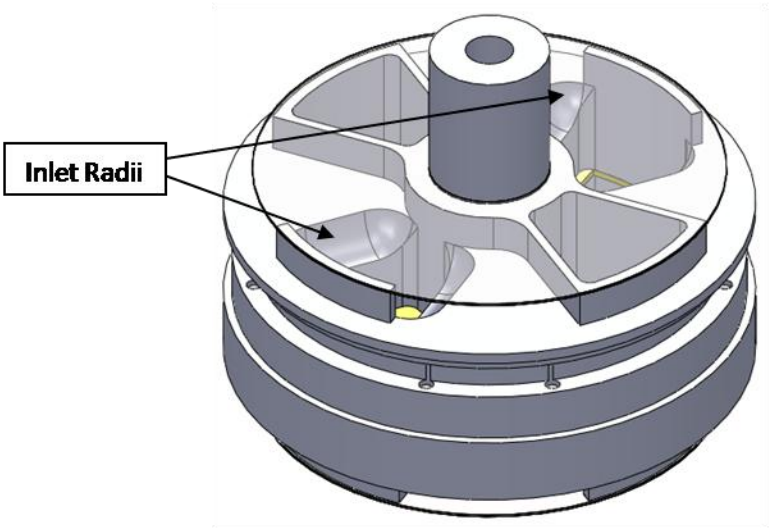

Figure 4.2 Isometric view of Final Prototype piston assembly

The purpose of this inlet geometry change is to reduce the minor losses associated with the piston geometry and increase the total force range of the damper.

4.2 Disc Valve Designs

Due to the difficult nature of modeling the fluid dynamics at and around the disc valve, an empirical approach was used to design the third and fourth iteration disc valve designs. First a test disc was designed. Figure 4.3 shows the top view cutout pattern of the disc used for the third iteration valve design.

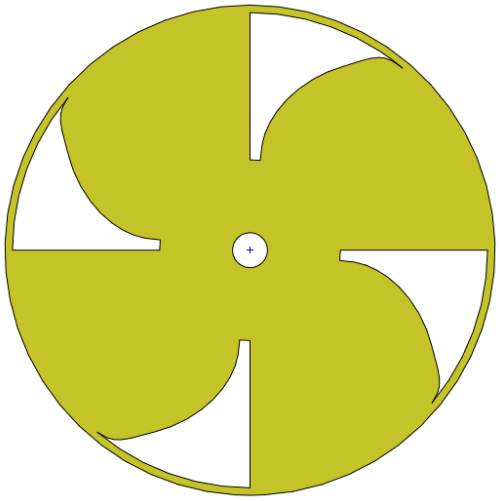

Figure 4.3 Test disc used to design third iteration valve

The test disc was designed with geometry similar to the second iteration disc. This new disc was tested and an area vs. peak force plot was generated for the Final Prototype damper. This relationship is shown below in Figure 4.4.

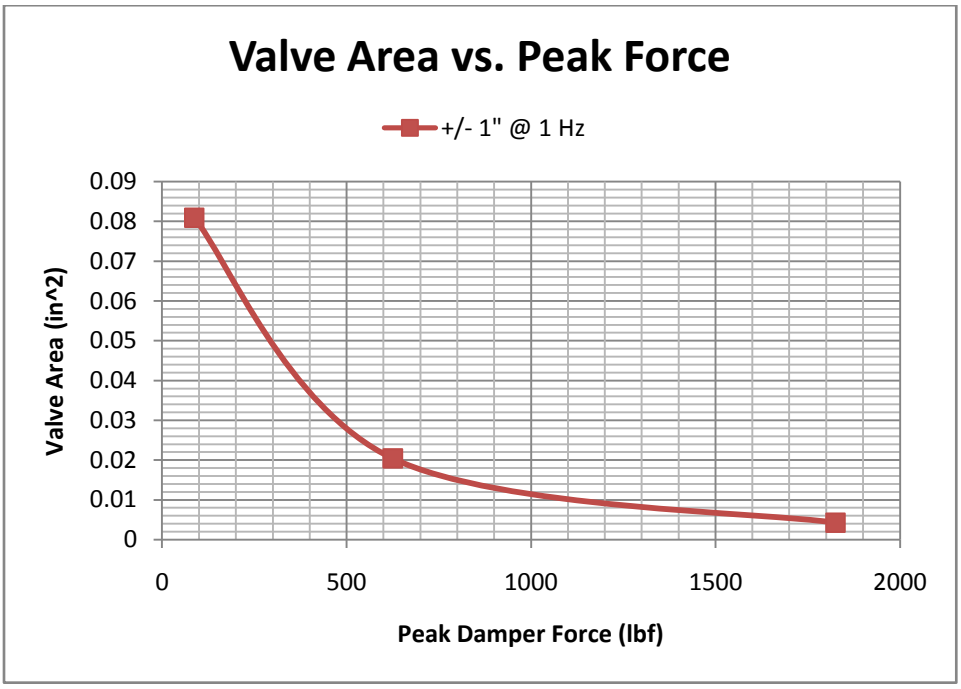

Figure 4.4 Valve area vs. peak force for Final Prototype damper with test disc

Using the area and force relationship determined through testing, a new disc was designed to effectively linearize the change in damping as a function of disc position. Only three data points were acquired from the test disc results that met the force range requirements. Interpolation of the valve area and peak force relationship, combined with estimations of force vs. valve area trends, seen in the first generation damper, served as a basis for third iteration disc design.

4.2.1 Third Iteration Disc Design

The third iteration disc orifice design was based on the force vs. area results obtained using the test disc. The third iteration disc is shown below in Figure 4.5, along with a plot of the valve area vs. disc position in Figure 4.6.

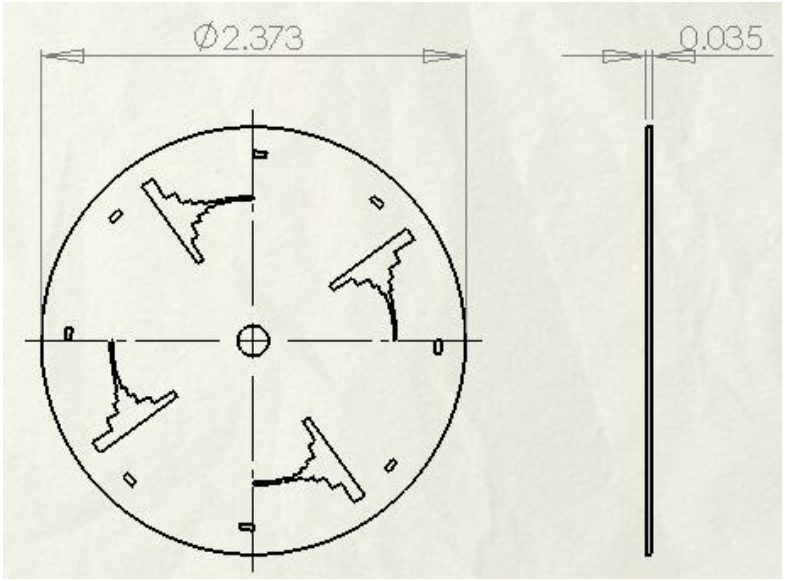

Figure 4.5 Third iteration disc design, front view and side views

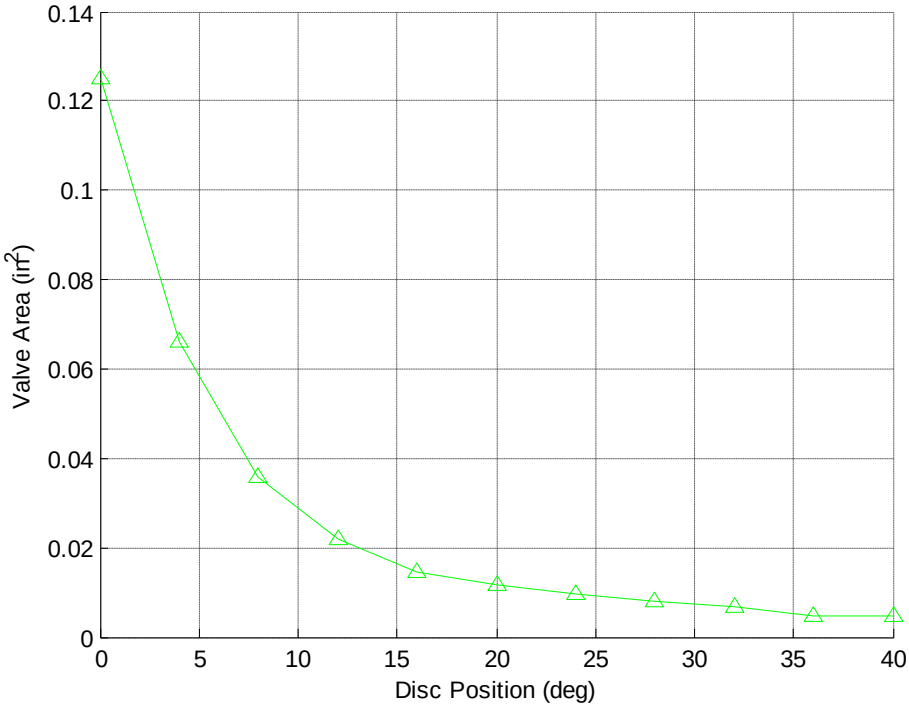

Figure 4.6 Third iteration valve area vs. disc position relationship

Figure 4.6 shows the third iteration valve area is drastically reduced in the first 10 degrees of rotation and the gradually tapered off between roughly 15 and 40 degrees. For ease of modeling, the disc was divided into ten discrete areas, each of which changes linearly as a function of rotation angle. One of these discrete areas is highlighted in Figure 4.7.

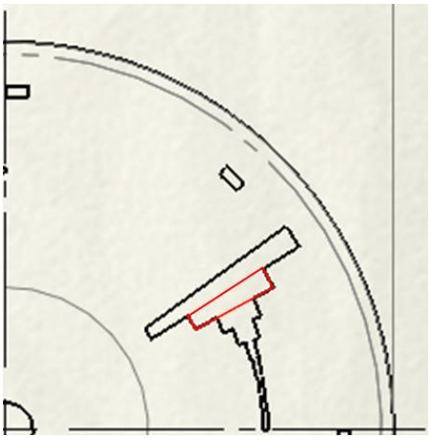

Figure 4.7 Close up of orifice area profile, discrete nature of orifice area design highlighted in box

4.2.2 Fourth Iteration Disc Design

The fourth iteration disc design is a spline interpolation of the third iteration design such that the change in orifice area is continuous with disc rotation. This design is shown in Figure 4.9 with a close-up of the orifice profile, including construction sketch lines, in Figure 4.8.

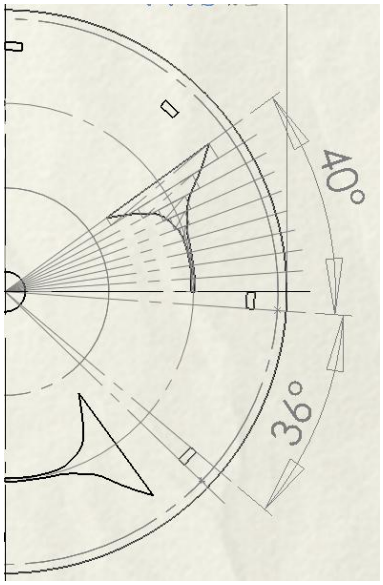

Figure 4.8 Close-up of orifice area profile, including construction line sketch, fourth iteration disc design

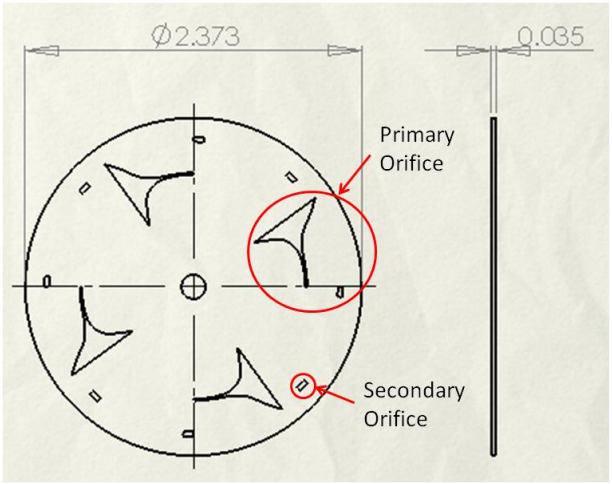

Figure 4.9 Fourth iteration disc design, front view and side views

Both fourth and third iteration disc designs are configured such that they can never be fully closed. A secondary orifice is opened as the primary orifice is closed, thus limiting the total force generating capability of the damper and protecting the internal components in the event the disc becomes uncontrollable. The secondary orifices and primary orifices are highlighted in Figure 4.9. A plot of the valve area vs. disc position for the fourth iteration disc design is shown in Figure 4.10 and all four iterations of disc design are compared in Figure 4.11.

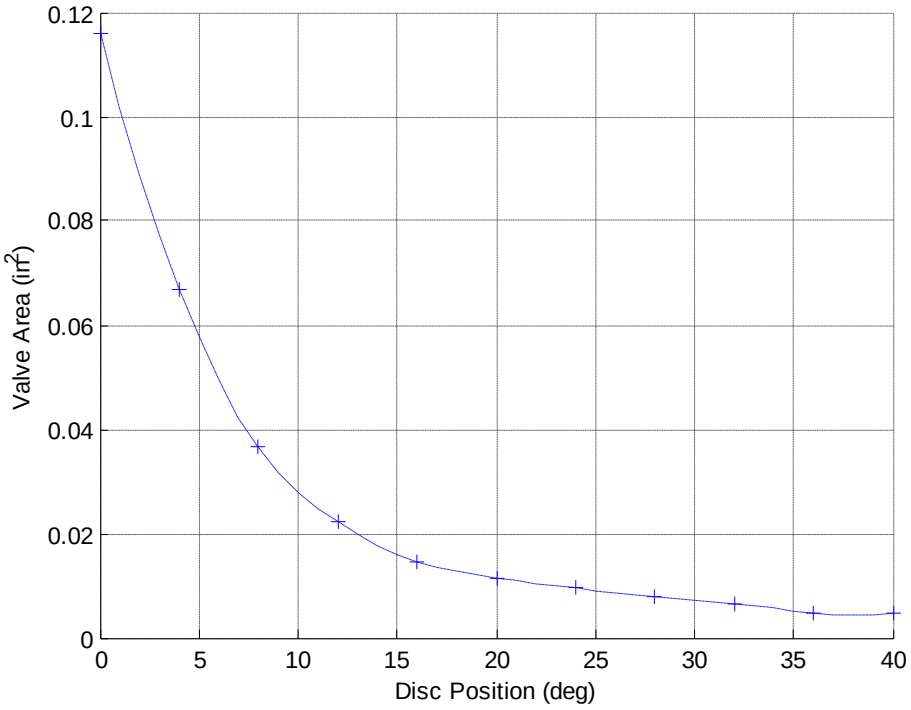

Figure 4.10 Fourth iteration valve area vs. disc position relationship

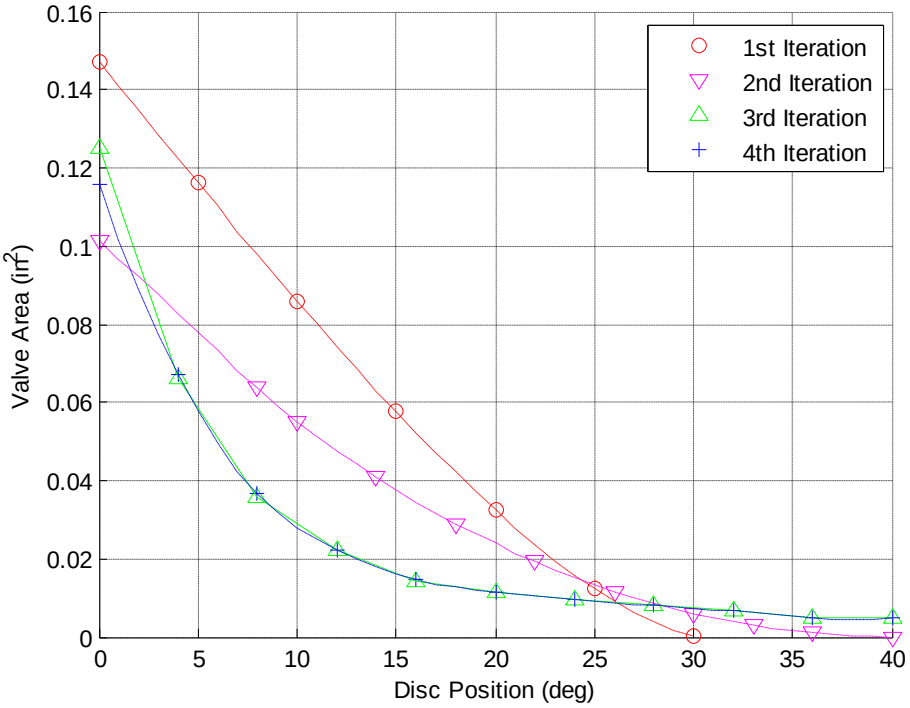

Figure 4.11 Comparison of orifice area vs. disc position for all four iterations

4.3 Notes on Fabrication

The piston halves were CNC machined from 6061 aluminum and the internal discs were laser cut from 316 stainless sheet. There were some problems with the laser cutting of the fourth iteration disc specifically. When converting to a DXF some of the resolution of the spline was lost and the laser cutter would travel linearly between sketch points instead of following the spline path. This was less of a problem with the third iteration disc due to the discontinuous nature of the orifice sketch. In either case, a higher precision laser cutter should be used for further development of disc valves.

The control rod is AISI 1566 steel case hardened to a depth of 0.027 inches, with a surface finish of approximately 12 R_q and a straightness tolerance of 0.002 inches per foot. The guide rod seal was originally a buna o-ring, but this caused significant friction and resistance to movement. Extrusion was also an issue and assembly typically caused damage to the o-ring,

leading to leaking issues. The top piston half was modified to accept a spring loaded graphite filled PTFE dynamic lip seal from Parker Hannifin Corp. The seal profile is shown in Figure 4.12. The gland dimensions are shown in Figure 4.13.

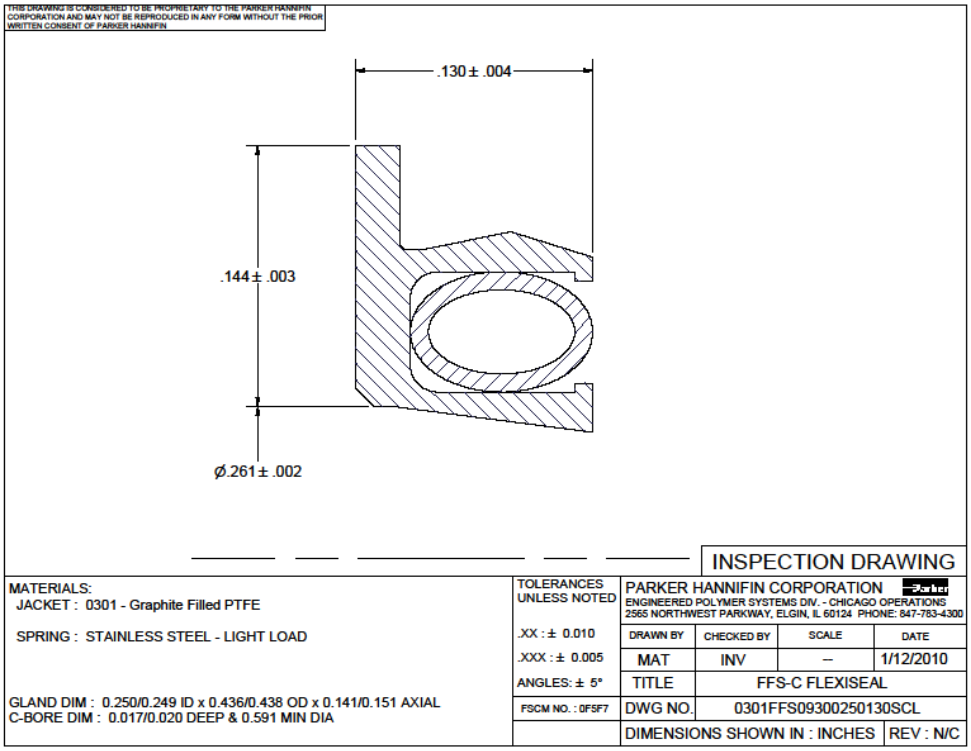

Figure 4.12 PTFE lip seal profile inspection drawing

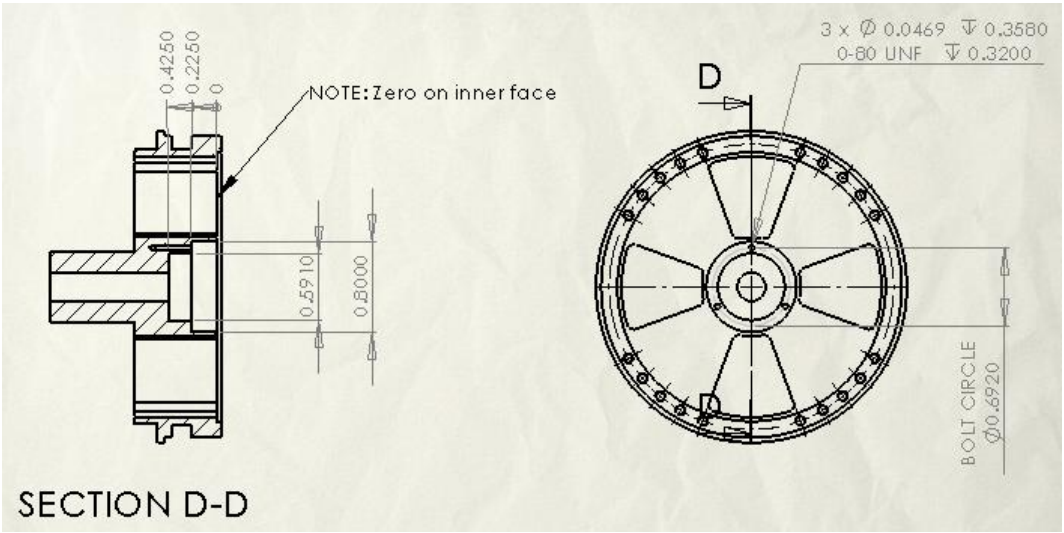

Figure 4.13 Bottom view of top piston half including section view with gland dimensions

Chapter 5

Final Prototype Mechanically Adjustable Hydraulic Damper Characterization

This chapter is concerned with the testing of the Final Prototype mechanically adjustable hydraulic damper and force characterization and analysis of the collected test data.

5.1 Third Iteration Experimental Setup

Tests were performed on a MTS 810: Material Test System load-frame, with a 5500 lb load cell, as shown in Figure 5.1.

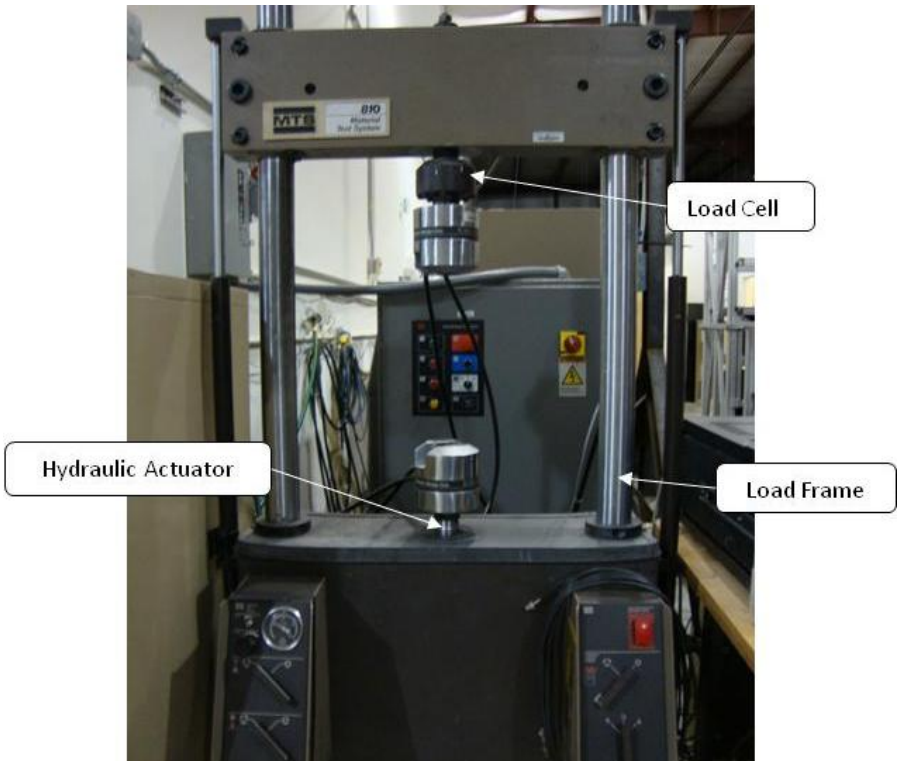

Figure 5.1 MTS load frame used in full scale damper tests

The MTS 810 is controlled with a 458.20 Micro-Console programmable controller (Figure 5.2). Data taken from the load cell is logged on a dedicated PC via a virtual instrument in a dSPACE environment.

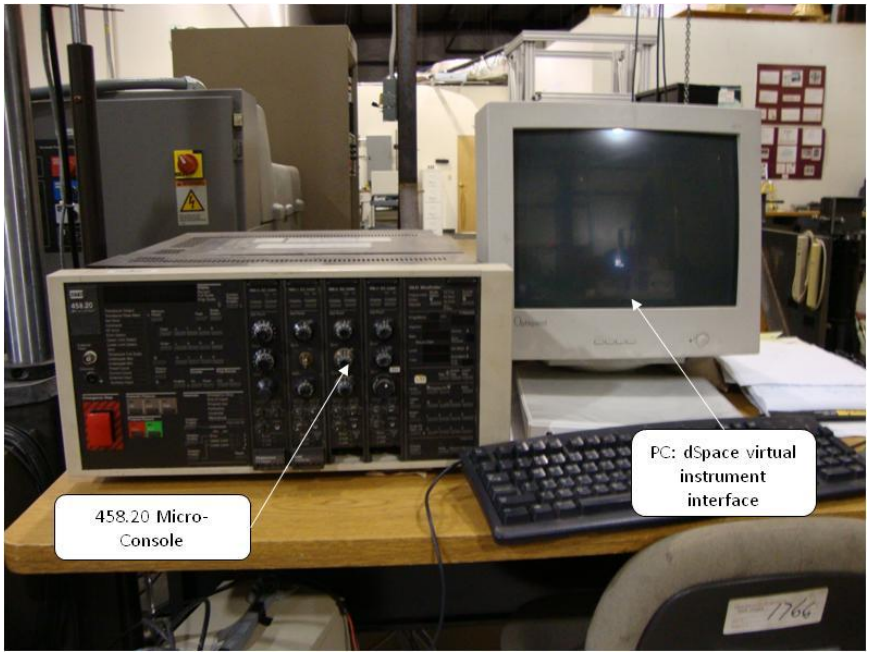

Figure 5.2 458.20 Micro-Console controller and dSPACE PC

5.2 Third Iteration Disc Test Results

Unlike the second iteration changes, the new disc design has a significant and beneficial impact on the force vs. disc position relationship. Figure 5.4 shows the test results for the third iteration disc design. The first four curves represent the damper response for a 1 Hz sine input. The damper began to cavitate in compression only, therefore the input waveform was changed. The next four tests were conducted at 0.1 Hz in compression and 1 Hz in rebound. This displacement input waveform is the summation of two haversine waves, shown in Figure 5.3.

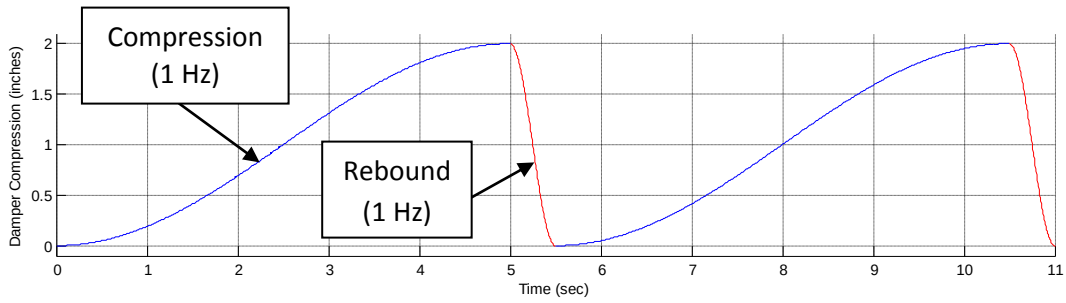

Figure 5.3 Displacement input waveform used for third and fourth iteration tests

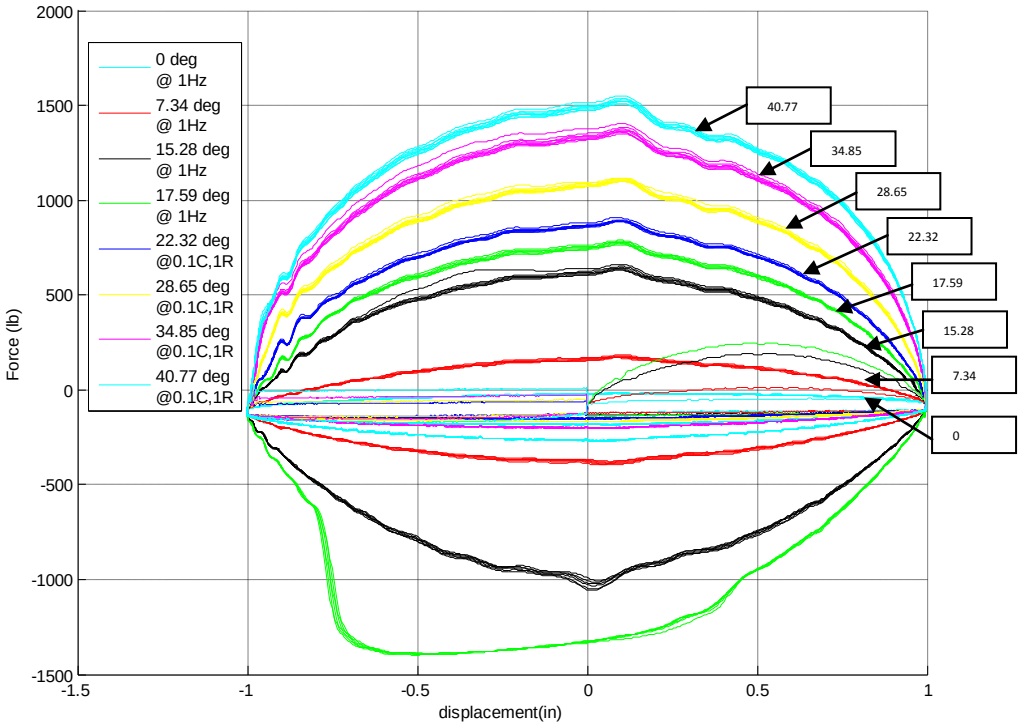

Figure 5.4 Force vs. displacement plot for Final Prototype damper, third iteration disc design

The legend on Figure 5.4 also corresponds to the force vs. velocity plot of Figure 5.5.

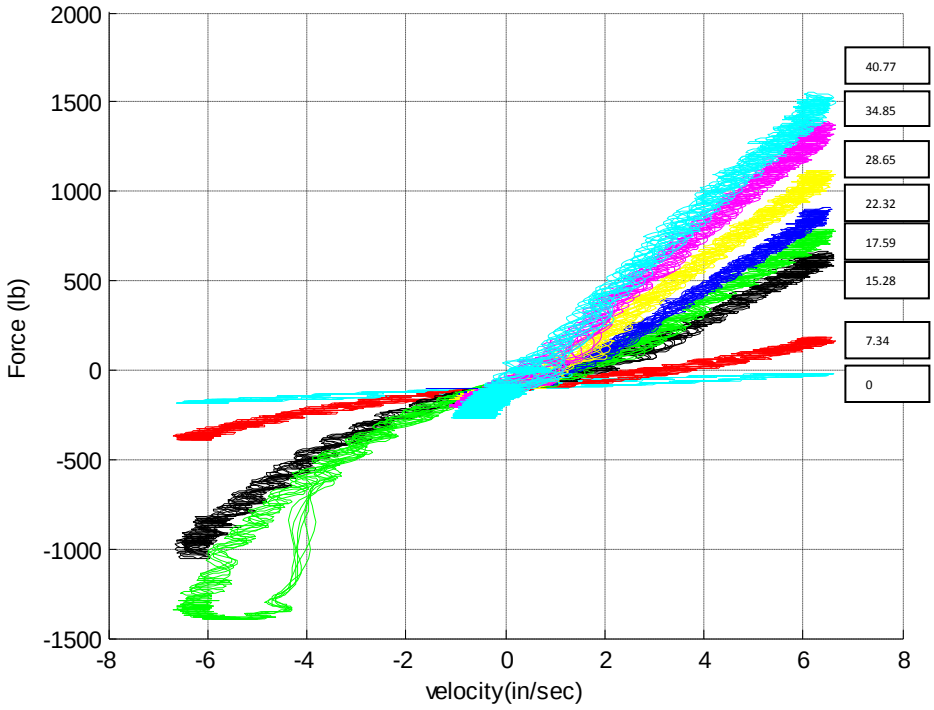

Figure 5.5 Force vs. velocity plot for Final Prototype damper, third iteration disc design

The rebound side (first quadrant) of Figure 5.5 shows the distinct and constant damping ratios achievable at different valve settings with the second generation damper. This test shows our final design offers a very large range of achievable damping ratios each with a predominantly linear response between 0 and 6 inches per second. The test data shown above was conducted at roughly 200 psi of gas pressure, effectively limiting compression force to approximately 1400 *lb* of force due to cavitation. Compression damping could be increased by increasing the gas pressure, or by adding a base valve in the damper body. The rebound side showed a range of 22 to 1 in peak force when normalized by peak force in the zero or "off state."

The improvements made in valve sensitivity are highlighted in Figure 5.6. Figure 5.6 is similar to Figure 23, but it also includes the results for the third iteration valve design and the desired valve characteristics.

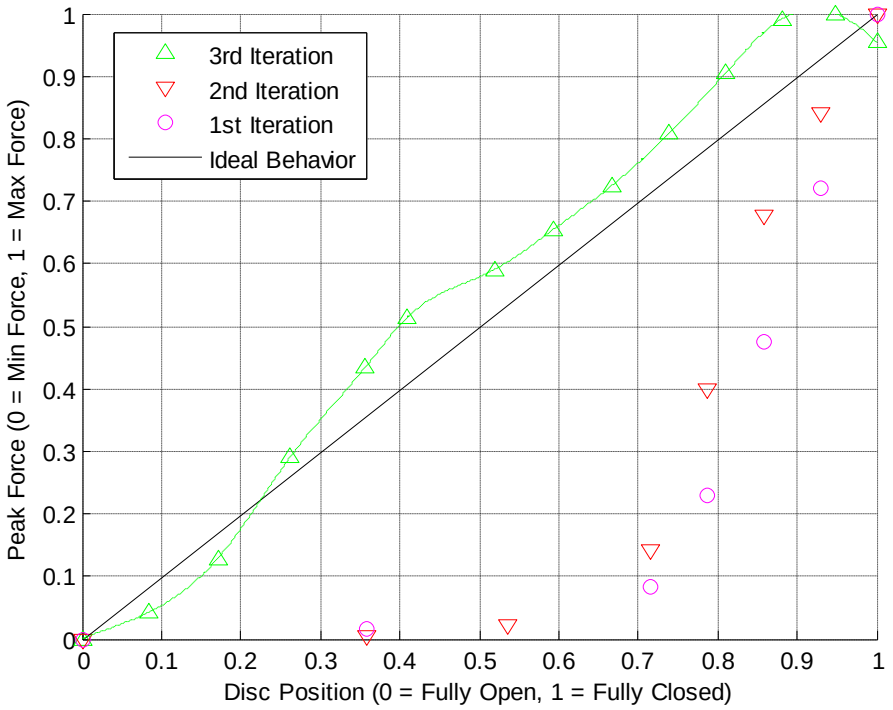

Figure 5.6 First, second, and third iteration comparison plot: normalized peak force vs. disc position relationship

Figure 5.6 illustrates the significant gains made throughout the design iterations across two generations of damper. The third iteration disc design exhibits nearly ideal response in terms of valve sensitivity. Peak force vs. disc position has a nearly linear relationship, which correlates well with our ideal response outlined in the Section 3.4.

5.2.1 Third Iteration Design Problems

Initial Tests of the Final Prototype mechanically adjustable hydraulic damper revealed some compliance issues with regard to the piston assembly. The piston halves were originally joined by eight 3-48 stainless steel socket head cap screws. Due to the unexpectedly high forces seen in rebound during higher frequency tests, these machine screws saw axial tensile loads beyond their yield strength. Before yielding however, the axial loading on these screws during testing opened up a radial leak path for hydraulic oil to bypass the disc valve and flow around the piston. This caused a significant reduction in damper force that will be discussed further in the next section. After repeated testing, the machine screws eventually failed and the piston halves were broken apart. The test results during failure are included in Figure 5.7, with bolt fracture occurring when the disc was 28.6 degrees closed. The failure resulted in a controller underpeak fault which aborted the test.

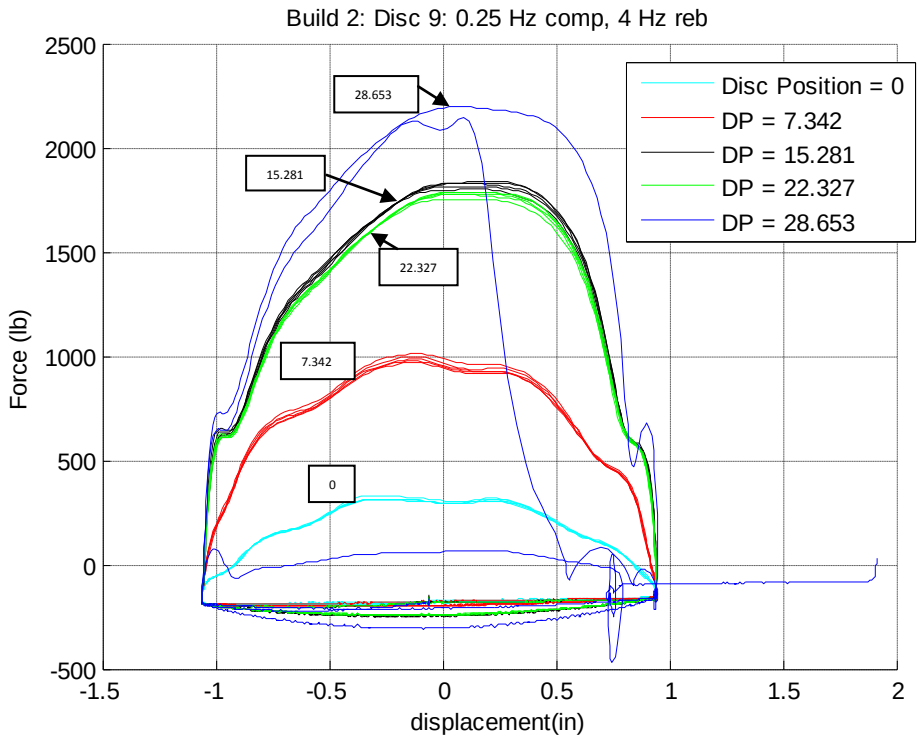

Figure 5.7 Machine screw failure during high frequency rebound tests

No damage was done to any of the piston components, and the piston halves were modified to accept 16 machine screws, doubling the number of fasteners of the original design.

5.3 Fourth Iteration Disc Test Results

After fixing the compliance issues experienced with the third iteration testing, the fourth iteration disc tests showed great improvement in force range. The input waveform shown in Figure 5.3 was used in the tests shown in Figures 5.8 and 5.9.

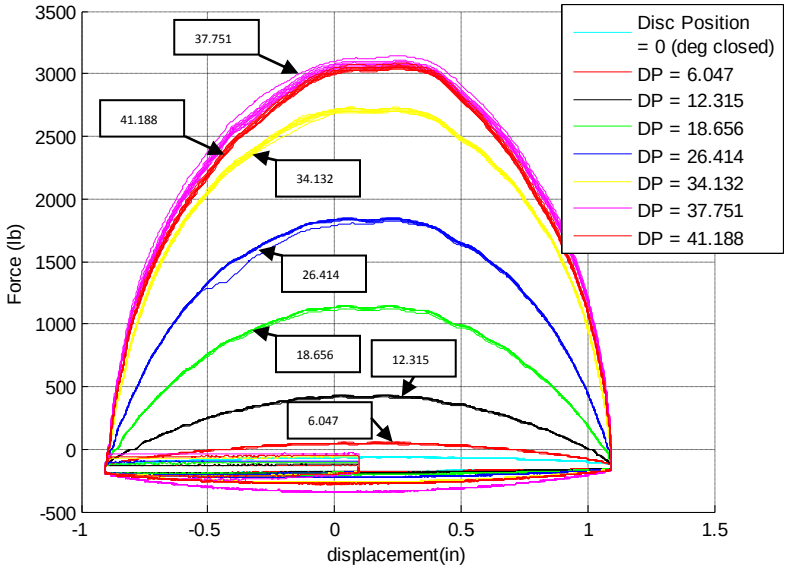

Figure 5.8 Force vs. displacement plot for the Final Prototype damper, fourth iteration disc design

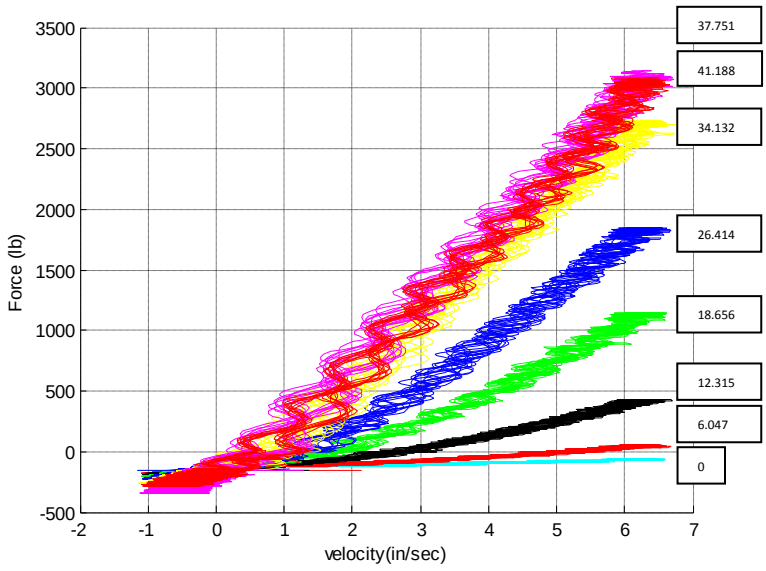

Figure 5.9 Force vs. velocity plot for the Final Prototype damper, fourth iteration disc design

The fourth iteration tests showed a significant increase in peak force at no cost to off-state (0 degrees valve closure) force. The gain in force range was also made at little cost to the sensitivity and the linearity of the valve response. The normalized peak force vs. normalized valve closure is plotted in Figure 5.10.

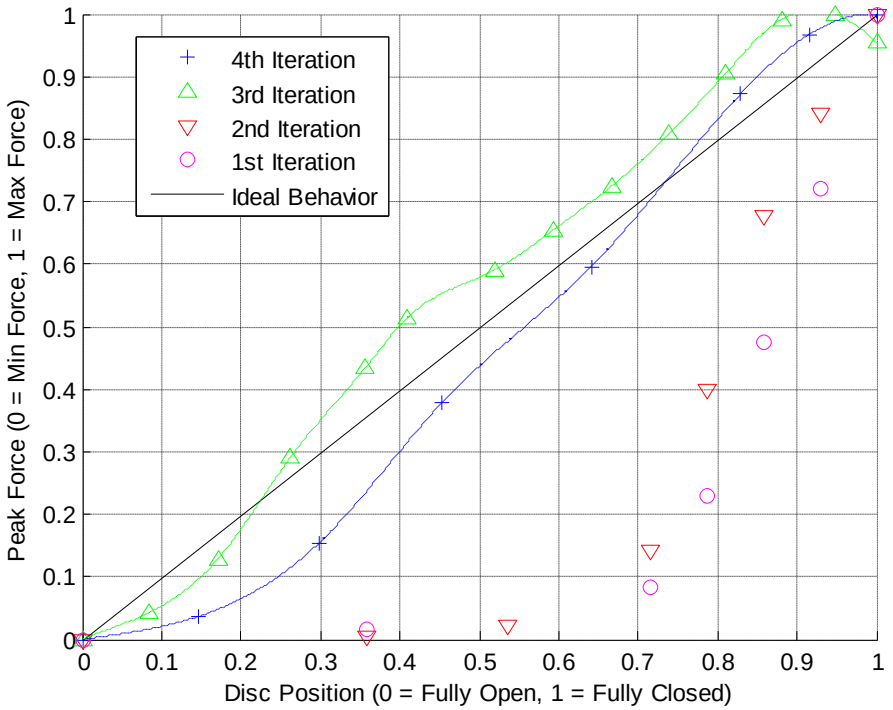

Figure 5.10 First, second, third, and fourth iteration comparison plot: normalized peak force vs. disc position relationship

Table 5.1 shows the gains in force range across all four iterations. The right hand column contains the normalized rebound force range for each damper tested at 1 Hz. This ratio is obtained by dividing the peak force generated (valve fully closed) by the minimum force generated (valve fully open), yielding an expression for force range that can be used to compare any semi-active damper, MR or electro-mechanical.

Table 5.1 Force range improvements throughout design iterations

Disc Design (Iteration)	Normalized Rebound Force Range @ 1 Hz
1st	5:1
2nd	9:1
3rd	19:1
4th	44:1

The gains in force range are even more significant in light of the simultaneous improvements in valve sensitivity. These gains will be further discussed in Chapter 6, a comprehensive comparison of MR dampers and mechanically adjustable hydraulic dampers for heavy truck applications.

5.4 Design Modularity and Implications

Because of the modular nature of the prototype dampers, they may be easily customized for different applications. The characteristics of the valve may be changed entirely by replacing the inner disc, a very inexpensive part even in low production runs. To demonstrate the importance of this cross platform versatility, an asymmetric damping concept is introduced.

By implementing an asymmetric disc valve, the ratio of rebound and compression damping can be changed entirely. Figure 5.11 shows a disc design for the asymmetric damping concept.

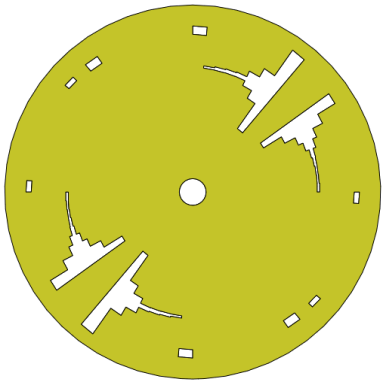

Figure 5.11 Asymmetric damping design concept

With the third and fourth iteration designs, disc rotation caused an increase or decrease in both rebound and compression force. The asymmetric design results in an inverse relationship between rebound and compression. As rebound orifice area is closed, compression area is opened. Figure 5.12 shows the change in orifice area with disc rotation.

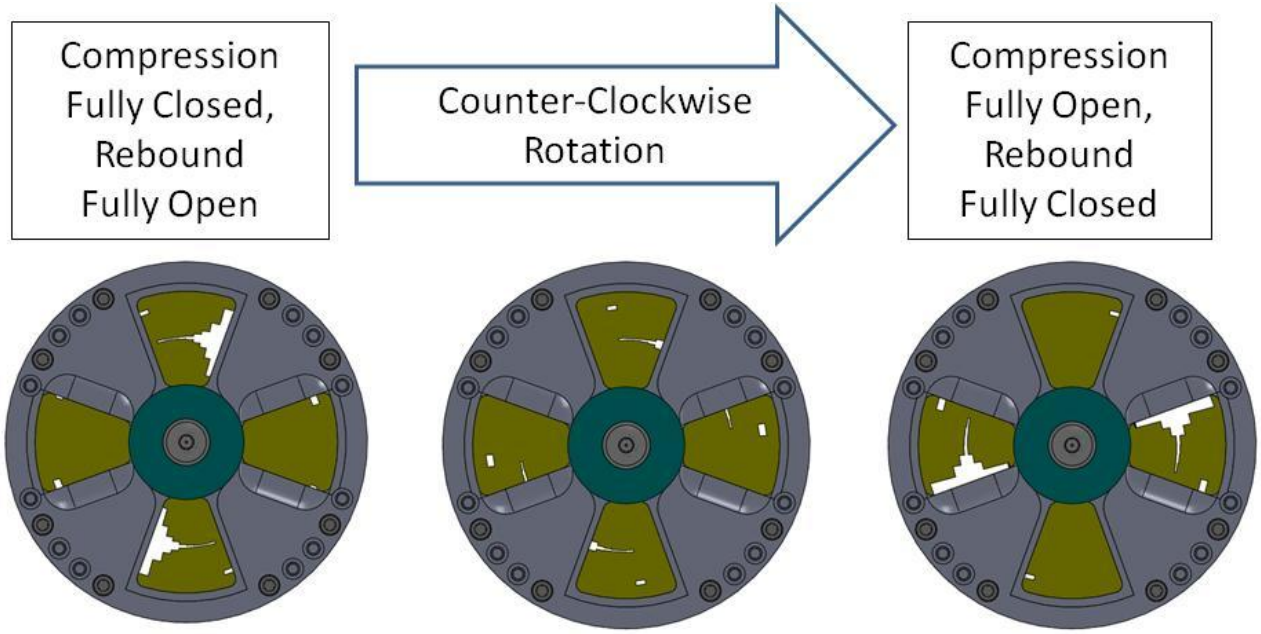

Figure 5.12 Asymmetric damping adjustment range

The goal of this design is to reduce the actuator requirements and reduce the power consumption of the damper for a control scheme such as skyhook control. Because the ratio of compression to rebound damping can be changed with disc position, in most cases the disc position needs only to be varied in relation to the state of the sprung mass, instead of the unsprung mass. This is

significant because, for larger vehicles, the sprung mass natural frequency is much lower than the unsprung mass natural frequency. This reduces the speed at which the actuator must move the disc, and reduces power consumption by requiring less disc motion to achieve the desired attenuation. This simple asymmetric disc design demonstrates the potential of the modular piston assembly design and the capability of the damper to be easily adapted to both physical systems and control schemes.

Chapter 6

Heavy Truck Applications of Electro-Hydraulic Dampers

Although electro-hydraulic mechanically adjustable dampers have been largely ignored in recent literature and study of semi-active suspension systems, their use is still intriguing for many applications. Some such voice coil dampers have enjoyed commercial success and remain on the market today. Other designs, such as the damper presented in this thesis, offer the potential to outweigh the benefits of an MR solution. The following sections will compare the prototype dampers introduced earlier with existing MR solutions, in light of heavy truck applications.

6.1 Dynamic Characteristics and Applications

The force range of an MR damper is dependent on many design considerations, including annular gap size or other orifice size, magnetic field strength, magnetic circuit design, as well as the particular MR fluid chosen for the damper. In general, however, the ratio of full on-state (max current or fluid saturation) to off-state (zero current) force is no greater than 8:1. Sahin, et al. [8] obtained approximately 8000 N when fully activated, versus 3000 N at zero current. Although this damper was designed to exceed the OEM passive damper during off-state, the normalized force range of 2.66:1 is worth noting. Poyner [5] obtained force ranges of approximately 4:1 and 7:1 for two MR dampers tested on a large SUV. Dogruer and Gordaninejad [15, 16] obtained approximately 2.3:1 for their HMMWV damper with shims. Mcmanus, et al. [14] obtained a normalized force range of approximately 6:1 during their testing of the *Motion Master semi-active damping system*, a commercially available damper manufactured by Lord Corporation. A summary of the normalized force ranges for the MR dampers discussed above is shown in Table 6.1.

Table 6.1 Force range comparison table

Author/Researcher	Normalized Force Range (Max/Min:1)
Sahin, et. al	2.7:1
Poyner	4:1
Poyner	7:1
Dogruer, et. al	2.3:1
Mcmanus, et. al	6:1

Comparing a typical MR damper of significant force range, 6.5:1 for example, with the Final Prototype damper reveals how much more control authority the Final Prototype damper has. Figure 6.1 shows the normalized force velocity characteristics of a typical MR damper compared with the Final Prototype damper introduced in chapter 4. The larger shaded region represents the total force range of the Final Prototype damper, while the smaller region represents the force range of a typical MR damper.

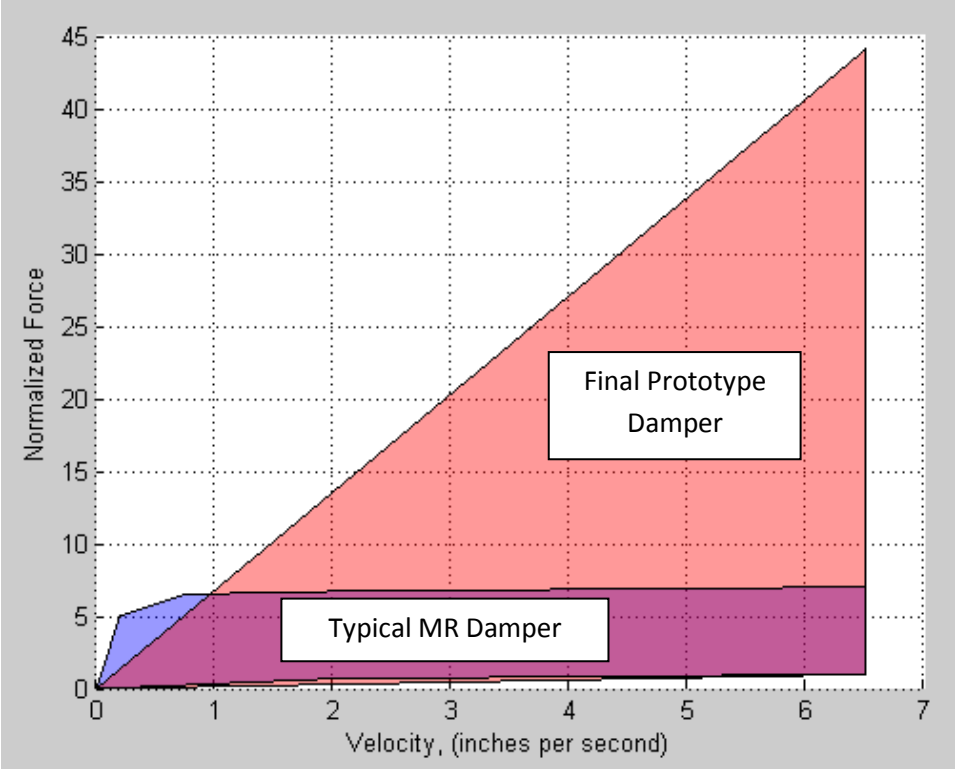

Figure 6.1 A comparison of normalized damper force vs. velocity for the Final Prototype damper and a typical MR damper

Figure 6.1 shows how much more control authority the Final Prototype damper has when compared with a typical MR damper. The implications of this increased force generating capability are non-trivial, particularly from a vehicle stability perspective.

6.1.1 Idealized Skyhook Control

Taking Skyhook control as an example, (6-1) contains the governing equations for skyhook control

$$\begin{cases} V_1 V_{12} > 0 & F_{sa} = G_s V_1 \\ V_1 V_{12} < 0 & F_{sa} = 0 \end{cases} \tag{6-1}$$

where V_1 and V_{12} are the absolute velocity of the sprung mass and the relative velocity across the suspension respectively, F_{sa} is the skyhook damping force, and G_s is the gain necessary to ensure the full range of the damper is used [17]. When the sprung mass and relative velocity have the same sign, the control law calls for a velocity proportional damping to limit the motion of the sprung mass. A larger force range allows the maximum amount of damping required to resist this sprung mass motion while still minimizing the off-state damping. Given some arbitrary maximum damping required for a skyhook controlled vehicle, the larger force range of the Final Prototype damper allows the physical system to more closely approximate the ideal case where $F_{sa} = 0$.

6.1.2 Heavy Truck Rollover

For heavy truck applications, the Final Prototype damper has potential to be very effective, particularly with regard to roll stability. Dahlberg et. al, identified roll stiffness and roll center height as the dominant parameters influencing Dynamic Rollover Threshold (DRT), a measure of the minimum absolute peak value of lateral acceleration causing vehicle rollover [18]. For low roll center vehicles the majority of lateral acceleration is transferred through the springs (elastic load transfer). These vehicles experience larger roll angles than vehicles with high roll

centers and more geometric load transfer. Trucks with changing payloads are also at risk of having larger center of gravity (CG) heights, which when combined with low roll centers and roll stiffness further decrease the DRT. These trucks are subject to a large lateral movement (Δy) of the center of gravity, as seen in Figure 6.2.

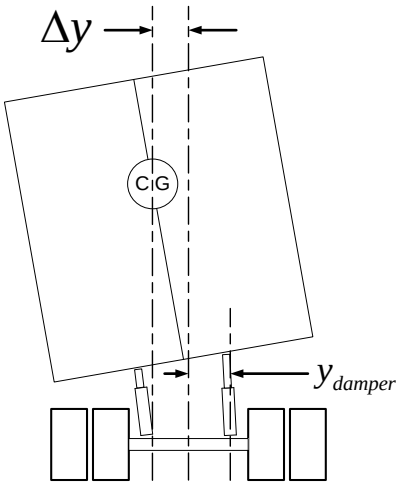

Figure 6.2 Truck roll diagram

Large trucks typically have dampers mounted far inboard on the axle, due to the width of the wheels and other packaging concerns. As the damper mounting location (marked as y_{damper} on Figure 6.2) decreases in length, the roll mode motion ratio decreases as well. This causes the roll mode to be grossly under-damped; resulting in large overshoots during transient maneuvers. Large Δy during transient maneuvers allows gravity to contribute a significant amount to the net roll moment on the vehicle, increasing the rollover risk. The dynamic force range of the Final Prototype damper presented in this study allows below critical heave damping for ride comfort, while still providing the force necessary to over-damp the roll mode, thus reducing overshoot and corresponding rollover risk.

6.2 Durability and High Temperature Functionality

For off road and military applications, the absorbed energy is significant enough to cause a large temperature change in the working fluid of the damper. This temperature change causes a

corresponding change in oil viscosity. High quality damper fluids are designed to limit the change in viscosity as a function of temperature, but this change is still significant. The fluid used in both prototype dampers is 5wt Silkolene oil, manufactured by Penske Corporation. This fluid has a viscosity index (VI) of 370. The exact change in viscosity can be calculated using the VI number and the initial viscosity (viscosity @ 40 degrees Celcius). For most high VI number oils ($350 < VI < 400$), the ratio of viscosity at 40 degrees divided by the viscosity at 100 degrees is approximately 3.2 (equation (6-2)).

$$\frac{\mu_{@40^{o}\,Celcius}}{\mu_{@100^{o}\,Celcius}} \approx 3.2 \tag{6-2}$$

Considering a linear damper with idealized laminar flow and force proportional to mean fluid velocity, the damping force will also be proportional to viscosity. Thus a 69% reduction (1/3.2) in viscosity will cause a proportional decrease in damper force.

Gordaninejad and Breese tested a variety of MR dampers and recorded peak force change with respect to time and temperature [9]. For the automotive MR fluid damper tested at 2 Hz and 1 cm amplitude, peak force decreased from 2000 N to approximately 1070 N, or 46.5%. Although the corresponding temperature data is not available for this test, it is reasonable to assume that the temperature change during this test was not greater than 60 degrees celcius. Thus in an absolute worst case scenario, the force reduction of the hydraulic damper will be approximately 22.5% greater in the hydraulic damper. Considering now that the Final Prototype damper has a normalized force range of approximately 44:1, even with poorer temperature and force characteristics, the Final Prototype damper retains a higher level of functionality in adverse conditions. The large normalized force range gives the damper more 'headroom' to cope with large changes in viscosity due to temperature extremes. Additionally, the actuator mechanism of the Final Prototype damper is located externally from the working fluid so as not to introduce any heat into the system. With MR dampers, the current flowing through the piston coil causes a temperature increase in addition to the viscous dissipation due to damper excitation. Notwithstanding the elegance of MR dampers, the Final Prototype damper has the potential to maintain higher levels of dynamic performance in long term, high temperature, and high power absorption applications.

Chapter 7

Concluding Remarks

During the course of this research, two prototype mechanically adjustable dampers were designed, built, and tested on an MTS dynamic material testing machine and a Roehrig EMA shock dynamometer. Force-velocity and force-displacement characteristics were acquired for all designs and used throughout the design development process. The following section will document the successes and failures of these dampers, and make recommendations for future studies.

7.1 Summary

7.1.1 Initial Prototype

The Initial Prototype damper served adequately as a proof of concept for the internal disc valve design. The thickness of the original disc caused significant fluid forces on the valve so the disc was redesigned accordingly. The new disc worked reasonably well, although the geometry of the valve was not ideal due to sensitivity issues. The second iteration disc valve design did not meet the goal of reducing the sensitivity and linearizing the force output with respect to disc position. This is due primarily to leaking and compliance issues in the first iteration design. The compliance induced leak paths skewed the orifice area and damper force relationship such that designing second iteration valves based on an estimate of disc position and corresponding orifice area of the first iteration design was flawed. The second iteration design changes did succeed in increasing the dynamic force range of the damper through the elimination of leak paths and improved fitment between components. The knowledge gained throughout the development of the Initial Prototype proved exceptionally valuable during the Final Prototype design process.

7.1.2 Final Prototype

The Final Prototype damper was designed to provide increased force range and improved sensitivity over the Initial Prototype. The friction on the disc valve control rod and the sealing of this rod proved to be significant hurdles throughout the development process. The buna o-ring used in the Initial Prototype proved to be ineffective in the Final Prototype design and susceptible to damage during assembly. Additionally, the o-ring seal caused excessive friction on the damper rod that tended to worsen as gas reservoir pressure increased. Significant effort was put into testing and choosing a new dynamic seal suitable for the pressures and surface finishes of the damper components. The new seal successfully reduced the friction and allowed the servo to turn the valve with little to no leaking (on the order of one drop per day).

Both third and fourth iteration disc designs proved successful; the latter providing an outstanding force range that exceeded our original goals. The Final Prototype damper exhibited nearly linear peak force versus disc position for both third and fourth iteration disc designs. The damper generates a normalized force range of 44:1, which is an order of magnitude higher than typical large vehicle MR dampers. The Final Prototype design shows the potential to be more effective than MR dampers for controlling undesirable chassis motions of low roll center, high CG heavy trucks.

7.2 Future Work and Design Recommendations

It is the hope of the author that additional testing will be conducted to prove the viability of the Final Prototype damper as an effective semi-active device. A new experimental setup and additional testing is required to gain further information about the fluid forces on the valve and the response time of the valve. The current design does not have a fully optimized actuator. The valve response time from fully closed to open is approximately 80 milliseconds. This puts the Final Prototype damper somewhere between a true semi-active and an adaptive device. Further optimization of the actuator used to operate the internal disc could dramatically improve the response times of the valve.

Additionally, the asymmetric damping disc design shows great potential for skyhook control applications. It is the hope of the author that this particular valve design will be tested in a quarter car rig to test the effectives of the asymmetric disc as a means of reducing actuator requirements and increasing the dynamic bandwidth of the damper.

If another piston is designed, it is the recommendation of the author that significant focus be placed on reducing the friction between the internal disc and the inner piston faces. Surface finishes on the inner face should be given particular importance, and the pistons should be machined from a soft steel with good machining properties, such as 12L14, as opposed to aluminum. Also, thrust bearings should be incorporated on the inner diameter of the internal disc as well as the outer diameter.

References

1. Inman, D. J. (2008). *Engineering vibration* (3rd.). Pearson Education, Inc.

2. Dixon, J. C. (1996). *Tires, suspension, and handling* (2nd., p. 621).

3. Dixon, J. C. (1999). *The Shock Absorber Handbook* (2nd.). Wiley-Professional Engineering Publishing.

4. Milliken, W. F., & Milliken, D. L. (1995). *Race car vehicle dynamics, Volume 1*. SAE Publications Group.

5. Poynor, J. (2001). *Innovative designs for magneto-rheological dampers*. Master of Science Thesis, Department of Mechanical Engineering, Virginia Tech

6. Lord Corporation. *Designing with MR Fluids*. Lord Corporation Engineering note. Cary, NC.

7. Jolly, M., Bender, J., & Carlson, J. (1999). Properties and applications of commercial magnetorheological fluids. *Journal of Intelligent Material Systems and Structures*, *10*(1), 5–13.

8. Sahin, H., Liu, Y., Wang, X., Gordaninejad, F., Evrensel, C., Fuchs, a., et al. (2007). *Full-Scale Magnetorheological Fluid Dampers for Heavy Vehicle Rollover*. Journal of Intelligent Material Systems and Structures, 18(12), 1161-1167. doi: 10.1177/1045389X07083137.

9. Gordaninejad, F., and Breese, D. G. (1999). *Heating of Magnetorheological Fluid Dampers*. Journal of Intelligent Material Systems and Structures (Vol. 10, pp. 634-645). doi: 10.1106/55D1-XAXP-YFH6-B2FB.

10. Simon, D., and Ahmadian, M. (2001). *Vehicle evaluation of the performance of magneto rheological dampers for heavy truck suspensions.* Journal of Vibration and Acoustics, *123*(July), 365. doi: 10.1115/1.1376721.

11. Farjoud, A., Ahmadian, M., and Craft, M. (2009). *Mathematical modeling and experimental characterization of hydraulic dampers : effects of shim stack and orifice parameters on damper performance*. CVeSS Internal Publication (pp. 1-24).

12. Kitching, K., Cole, D., and Cebon, D. (2000). *Performance of a semi-active damper for heavy vehicles*. Journal of dynamic systems, measurement, and control, 122(September), 498.

13. Wolfe, P., Schwemmer, L., Prindle, D., and Tidwell, C. (1993). *Valving for a controllable shock absorber*. *US Patent*.

14. Mcmanus, S. (2002). *Evaluation of Vibration and Shock Attenuation Performance of a Suspension Seat With a Semi-Active Magnetorheological Fluid Damper.* Journal of Sound and Vibration, 253(1), 313-327. doi: 10.1006/jsvi.2001.4262.

15. Droguer, U. (2003). *Design and development of a magneto-rheological fluid damper for a high mobility multi-purpose wheeled vehicle (HMMWV.)*

16. Drogruer, U., Gordaninejad, F., and Evrensel, C.A. (2004). *A magneto-rheological fluid damper for a high-mobility multi-purpose wheeled vehicle (HMMWV).* Proceedings of SPIE, 5386, 195-203.

17. Ahamdian, M., Song, X., and Southward, S.C. (2004). *No-Jerk Skyhook Control Methods for Semiactive Suspensions.* Journal of Vibration and Acoustics, 126(4), 580.

18. Dahlberg, E., and Stensson, A. (2006). *The dynamic rollover threshold – a heavy truck sensitivity study.* The International Journal of Vehicle Design, 40(1/2/3), 228.

19. Hac, A. (2004). *Rollover stability index including effects of suspension design.* Progress in Technology, 724.

20. Sun, Y., and Parker, G. (1993). *A position controlled disc valve in vehicle semi-active suspension systems.* Control Engineering Practice, 1(6), 927-935.

21. Usman, A., and Parker, G. (1987). *A Low-Cost Electro-Hydraulic Proportional Valve.* The Journal of Fluid Control, 17(4), 55-76